Microscopic mechanisms of laser ablation of organic solids in the thermal and stress confinement irradiation regimes

Leonid V. Zhigilei[a] and Barbara J. Garrison[b]
Department of Chemistry, The Pennsylvania State University, University Park, Pennsylvania 16802

(Received 29 December 1999; accepted for publication 27 April 2000)

The results of large-scale molecular dynamics simulations demonstrate that the mechanisms responsible for material ejection as well as most of the parameters of the ejection process have a strong dependence on the rate of the laser energy deposition. For longer laser pulses, in the regime of thermal confinement, a phase explosion of the overheated material is responsible for the collective material ejection at laser fluences above the ablation threshold. This phase explosion leads to a homogeneous decomposition of the expanding plume into a mixture of liquid droplets and gas phase molecules. The decomposition proceeds through the formation of a transient structure of interconnected liquid clusters and individual molecules and leads to the fast cooling of the ejected plume. For shorter laser pulses, in the regime of stress confinement, a lower threshold fluence for the onset of ablation is observed and attributed to photomechanical effects driven by the relaxation of the laser-induced pressure. Larger and more numerous clusters with higher ejection velocities are produced in the regime of stress confinement as compared to the regime of thermal confinement. For monomer molecules, the ejection in the stress confinement regime results in broader velocity distributions in the direction normal to the irradiated surface, higher maximum velocities, and stronger forward peaking of the angular distributions. The acoustic waves propagating from the absorption region are much stronger in the regime of stress confinement and the wave profiles can be related to the ejection mechanisms. © *2000 American Institute of Physics.*
[S0021-8979(00)03715-4]

I. INTRODUCTION

The nature of the processes induced in a target material by pulsed laser irradiation is defined by the combination of the optical, mechanical and thermodynamic properties of the material as well as the laser parameters such as pulse duration and fluence. The analysis of the laser-induced processes becomes more complex as the laser pulse duration becomes shorter. The competition of the rate of the energy deposition with characteristic times needed for thermodynamic and mechanical response of the material to the fast laser heating determines the character and the relative importance of photothermal and photomechanical processes in laser ablation. In the present study we apply a molecular-level simulation technique to systematically investigate the collective processes leading to the material ejection at different laser fluences and pulse durations. The focus of this study is on the differences in the ejection mechanism in the irradiation regimes where photothermal and photomechanical processes dominate and on the implications of these differences on the practically important characteristics of the laser ablation.

There are a number of applications of laser ablation of organic solids where the short time of the energy deposition is critical. In particular, in an important mass spectrometry technique, matrix-assisted laser desorption ionization (MALDI), a short time during which large fragile biomolecules experience a high-temperature environment presumably provides the conditions that allow them to survive the desorption from a matrix of small absorbing molecules and to be detected as intact ions.[1–3] In laser surgery a short duration of the laser pulse allows one to restrict the energy deposition within the absorbing volume and minimize the collateral thermal damage.[4] The laser pulse duration, τ_p, in these applications is typically shorter than the time of dissipation of the absorbed laser energy by the thermal conduction, τ_{th}, the condition that is commonly referred to as *thermal confinement.*[5,6] The condition for thermal confinement can be expressed as $\tau_p < \tau_{\text{th}} \sim L_p^2/D_T$, where D_T is the thermal diffusivity of irradiated material and L_p is the laser penetration depth or the size of the absorbing structure.

The pulse duration in the regime of thermal confinement is usually shorter than the time needed for gas phase bubble formation and diffusion in the process of heterogeneous boiling.[7,8] As a result, the absorbing material can be overheated much beyond the boiling temperature, turning a normal surface evaporation at low laser fluences into an explosive vaporization, or phase explosion, at higher fluences.[6–10] An onset of massive material removal, or ablation, is defined in this case by the critical energy density sufficient for the overheating of the surface layer up to the limit of its thermodynamic stability.[6] It has been predicted, based on thermodynamic considerations, that phase explosion results in a spontaneous decomposition of the ejected plume into a two-phase system of gas-phase molecules and liquid droplets.[7–9]

[a]Present address: Department of Materials Science and Engineering, Thornton Hall, University of Virginia, Charlottesville, VA 22903; electronic mail: lz2n@virginia.edu
[b]Electronic mail: bjg@chem.psu.edu

The yield of individual molecules has been routinely measured in mass spectrometry postionization experiments,[11–15] while the ejection of nanometer-size clusters has been observed recently both experimentally[16–20] and in molecular dynamics computer simulations.[6,10,21–23]

In the absence of photochemical decomposition,[24,25] that involves a direct photodissociation of the molecular bonds and could be dominant in the deep ultraviolet, an explosive vaporization is likely to be a major mechanism of ablation of organic materials at sufficiently high laser fluences. There are, however, a significant number of experimental observations suggesting that ablation can be initiated at the energy densities much lower than those required for boiling and vaporization. Energetically efficient ablation has been reported for liquids,[26–28] polymers,[29] biological tissues,[30–32] and for organic matrixes used in infrared (IR)-MALDI.[33] A plausible explanation for the onset of ''cold'' laser ablation has been proposed based on consideration of photomechanical effects caused by laser-induced stresses.[30,34,35] The magnitude of the laser-induced stresses and the role of the associated photomechanical effects in material removal depends on the relation between the rate of energy deposition and the characteristic time of mechanical equilibration of the absorbing volume, τ_s. When the laser pulse duration is shorter or comparable to the time that is needed to initiate a collective motion of molecules within the absorbing volume, the laser heating takes place at nearly constant volume conditions, causing a high thermoelastic pressure buildup. This condition, usually referred to as inertial[10,30,36] or *stress confinement*,[5,26,27,32] can be expressed as $\tau_p \leqslant \tau_s \sim L_p/C_s$, where C_s is the speed of sound in the irradiated material.[37] It has been shown by a number of analytical calculations[27,34,36,38,39] that interaction of the compressive thermoelastic pressure, formed within the absorption region, with the free surface of the irradiated sample can lead to tensile stresses sufficiently high to cause mechanical fracture/spallation of a brittle material or promote cavitation in a metastable liquid. The coalescence of microcracks or cavities within the spallation region can lead to the mechanical disruption and ejection of large[39] and relatively cold pieces of material. This, in effect, should reduce the energy density needed for material removal well below the one for vaporization.

The evidence discussed above points to a strong dependence of the threshold fluence for the onset of ablation, the parameters of the ejected plume, and the character of the damage done to the target on the balance between the thermal and mechanical processes induced by laser irradiation. Therefore, it is highly desired to have a thorough understanding of both the involved physical processes and the conditions that define the transitions between different ablation regimes. Such an understanding would allow one to precisely tailor laser fluence, pulse duration, and wavelength dependent penetration depth to achieve a required experimental result. As discussed above, the conditions for thermal and stress confinement as well as some of the qualitative aspects of thermal and mechanical mechanisms of laser ablation are roughly understood. Information on microscopic mechanisms and the nature of the laser-induced processes at the submicron scale, however, is lacking.

A method that is capable of providing a detailed molecular-level description of the laser-induced processes is the molecular dynamics (MD) computer simulation technique. The direct application of the atomistic MD approach to the laser ablation phenomenon, however, is hampered by a collective character of the involved processes occurring at the mesoscopic rather than molecular scale.[3,40] Recent development of a coarse-grained breathing sphere MD model,[21] where a group of atoms rather than each atom is treated as a unit, has significantly expanded the time and length scales accessible for the simulations. The model not only allows one to perform simulations with irradiation parameters comparable to the experimental values,[6] but it also permits a translation of microscopic information on the dynamics of individual molecules into a mesoscopic description of the laser-induced processes in terms of temperature, pressure, and energy distributions within the irradiated sample.[10,21,41,42] In addition, large-scale simulations allow one to study the ejection of large clusters of material and to describe the ejected plume in terms of velocity and angular distributions.[43,44]

In the present work we focus on the dependence of the mechanisms of material ejection on irradiation conditions and, in particular, on the difference of the ablation mechanisms in the regimes of stress and thermal confinement. We perform two series of large-scale MD simulations for a range of laser fluences. The values of laser penetration depth and pulse width are chosen in order to make sure the regime of stress confinement is realized in one set of the simulations and the regime of thermal confinement is achieved in another. The description of the computational setup and the irradiation parameters is given in Sec. II. The fluence dependence of the total ablation yield is presented and related to analytic descriptions for laser desorption and ablation in Sec. III A. The analysis of the ejection mechanisms and the cluster composition of the ablation plume is given and related to experimental data and the existing theoretical models in Sec. III B. The yields of monomers and the velocity distributions of ejected molecules are given and related to mass spectrometry experimental data in Sec. III C. The profiles of the acoustic waves propagating from the absorption region are presented and related to piezoelectric measurements in Sec. III D. The comparative analysis of the overall pictures emerging from the simulation of laser ablation in the regimes of stress confinement and thermal confinement is given in Sec. IV.

II. COMPUTATIONAL SETUP

Here in Sec. II we review the basic features of the breathing sphere model developed for MD simulations of laser ablation of organic solids and discuss a dynamic boundary condition designed to simulate nonreflecting propagation of the laser-induced pressure wave through the boundary of the MD computational cell. Then we describe the computational setup and explain the choice of the irradiation parameters used in the present study.

A. The breathing sphere model

We give only a brief review here of the breathing sphere model that is described in more detail elsewhere.[21] The model assumes that each molecule (or appropriate group of atoms) can be represented by a single particle. The parameters of interparticle interaction are chosen to reproduce the properties of the material, in this case, a molecular solid. In order to simulate molecular excitation by photon absorption and vibrational relaxation of the excited molecules, an additional internal degree of freedom is attributed to each molecule. This internal degree of freedom, or breathing mode, is realized by allowing the particles to change their sizes. The parameters of a potential function ascribed to the internal motion can be used to change the characteristic frequency of the breathing mode and to affect the coupling between internal and translational molecular motions. In effect one can control the rate of the conversion of internal energy of the molecules excited by the laser to the translational and internal motion of the other molecules. The rate of the vibrational relaxation of excited molecules is an input parameter in the model and can be either estimated from experimental data[45] or modeled with atomistic[22] or *ab initio* molecular dynamics simulations.[46,47]

The laser irradiation is simulated by vibrational excitation of molecules that are randomly chosen during the laser pulse duration within the penetration depth appropriate for a given wavelength. Vibrational excitation is modeled by depositing a quantum of energy equal to the photon energy into the kinetic energy of internal motion of a given molecule. An alternative result of the photon absorption is photofragmentation, when an excited molecule reacts photochemically and forms fragments. An increase of the volume occupied by the reaction products can be simulated by either an increase of the equilibrium radii of spherical particles representing the excited molecules[21,48,49] or by introducing several smaller particles representing the reaction products.[50]

The total number of photons entering the model during the laser pulse is determined by the laser fluence, incident laser energy per unit surface area. The absorption probability can be modulated by Lambert–Beer's law to reproduce the exponential attenuation of the laser light with depth or can be restricted to a certain component within a complex material.

Since in this model each molecule is represented by a single particle, the system size can be sufficiently large to reproduce the collective dynamics leading to laser ablation and damage. Moreover, since explicit atomic vibrations are not followed, the time step in the numerical integration of the equations of motion can be much longer and the dynamics in the irradiated sample can be followed for as long as nanoseconds. One effect, however, that is difficult to simulate directly even within the coarse-grained breathing sphere MD model is propagation of the laser induced elastic wave. The method used to minimize the effects of the reflection of the wave from the boundary of the computational cell is discussed below.

B. Dynamic boundary condition

The generation of stress waves is a natural result of the fast energy deposition in the case of short pulse laser irradiation.[21,24,26–28,32,34,36,38,41,42,51] For a simulation with laser pulse duration of 15 ps, penetration depth of 50 nm, and fluence of 55 J/m^2 the formation and propagation of a plane pressure wave within the MD computational cell are shown in the form the pressure contour plots in Fig. 1. In this case the high pressure builds up in the surface region during the laser pulse and drives a strong compression wave into the bulk of the sample. Simulation of the propagation of the pressure wave requires the size of the MD computational cell to be increased linearly with the time of the simulation. For times longer than ~100 ps the size of the model required to follow the wave propagation becomes computationally prohibitive. If large computational cells are not used, however,

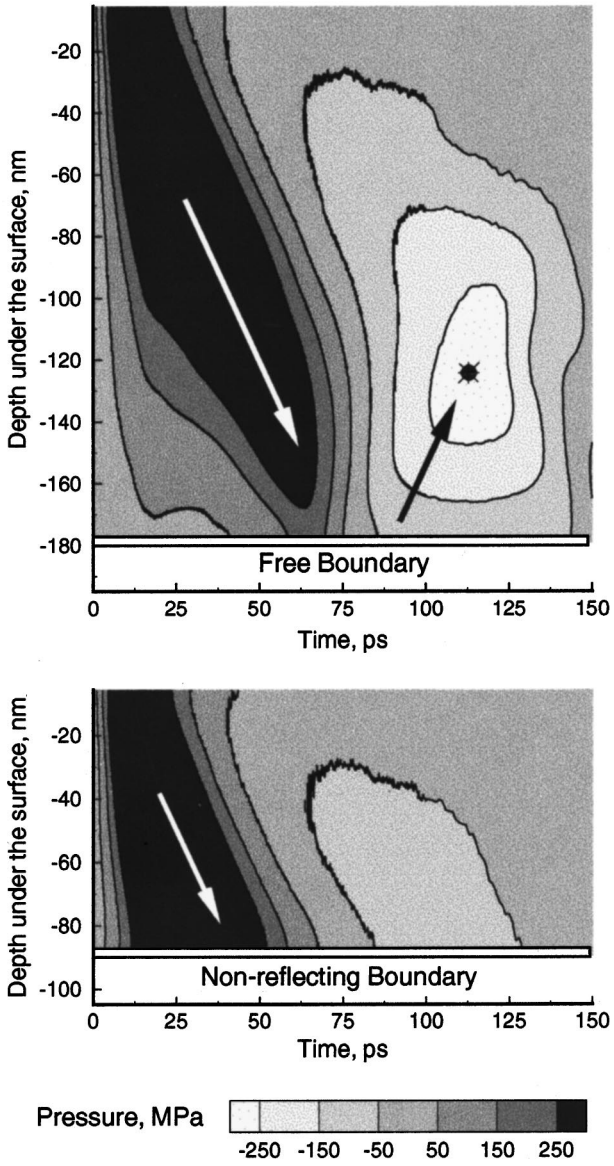

FIG. 1. Pressure contour plots for simulations performed for (a) computational cell of 10×10×180 nm and free boundary condition at the bottom of the computational cell and (b) computational cell of 10×20×90 nm and the dynamic nonreflecting boundary condition at the bottom of the computational cell. The laser penetration depth is 50 nm, the pulse duration is 15 ps, and the fluence is 55 J/m^2. The arrows show the direction of the pressure wave propagation. The depth and time of the mechanical damage caused by the reflected pressure wave are marked by (✸).

artificial border effects can interfere with the simulation results. Both rigid and free boundary conditions lead to the complete reflection of the pressure wave, as shown in Fig. 1(a) for the case of free boundary. This reflection of the pressure wave can cause the effect known as back spallation,[42] when the tensile strength of the material is exceeded and fracturing occurs at a certain depth near the back surface of the sample. The reflected wave can also reach the front surface of the irradiated sample and contribute to the material ejection.

In order to avoid artifacts due to the pressure wave reflection, we have developed a simple and computationally efficient boundary condition based on analytical evaluation of the forces acting at the molecules in the boundary region from the outer ''infinite medium.''[42] In this approach the boundary condition is a set of terminating forces that are applied to the molecules in the boundary region. In the calculation of the terminating forces, that are updated at each integration step, we take into account three effects, namely, the static forces that mimic interaction with molecules beyond the computational cell, the forces due to the direct laser energy absorption in and around the boundary region during the laser pulse, and the forces due to the pressure wave propagation through the boundary region. The contribution of the pressure wave to the terminating force is calculated based on the traveling wave equation and is proportional to the instantaneous velocity of the boundary.[42]

As shown in Fig. 1(b), the dynamic boundary condition allows us to simulate nonreflective propagation of the pressure wave through the boundary of the MD computational cell and to restrict area of the MD simulation to the region where active processes of laser-induced melting, ablation, and damage occur. An alternative approach to the problem of pressure wave reflection is to combine the MD model with the continuum finite element method.[52,53] The advantage of this approach is the capability to study the long-range propagation of the waves and their interaction with other MD regions of a large system.[53] In the present work, however, the aim is merely to avoid artifacts due to the pressure wave reflection and a simple and computationally efficient boundary condition described above appears to be sufficient.

C. Simulation setup

The system chosen for modeling of laser ablation is a molecular solid or matrix used in mass spectrometry MALDI experiments. The parameters of the intermolecular potential are chosen to represent the van der Waals interaction in a molecular solid with the cohesive energy of 0.6 eV, elastic bulk modulus of ~ 5 GPa, and density of 1.2 g/cm^3. A mass of 100 daltons is attributed to each molecule. An amorphous molecular solid prepared by melting of a close packed crystal and subsequent quenching from the melt[54] is used in the simulation.[21]

A schematic sketch of the simulation setup is shown in Fig. 2. Most of the results are obtained using a computational cell with dimensions of $10\times10\times100$ nm (70 526 molecules). A few test simulations with larger computational cells, $20\times10\times100$ nm (141 052 molecules), $40\times10\times90$ nm

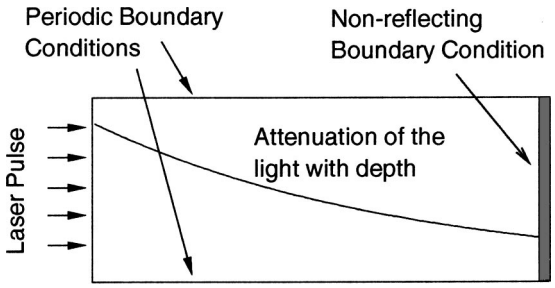

FIG. 2. Schematic sketch of the simulation setup.

(253 808 molecules), and $10\times10\times180$ nm (126 950 molecules), are performed in order to make certain that the simulation results are not affected by the finite size of the computational cell. Periodic boundary conditions in the directions parallel to the surface are imposed. These conditions simulate the situation in which the laser spot diameter is large compared to the penetration depth so that the effects of the edges of the laser beam are neglected. At the bottom of the MD computational cell we apply the dynamic boundary condition described in Sec. II B.

D. Irradiation regimes

The laser irradiation at a wavelength of 337 nm (3.68 eV) is simulated and an exponential decrease of the absorption probability with depth in accordance with Beer's law is applied. An absorption depth used in the simulations, 50 nm, is in the range of the values appropriate for strongly absorbing matrixes used in ultraviolet (UV)-MALDI.[55] The values of the laser pulse duration, 15 and 150 ps, are chosen in order to make sure that simulations are performed in two distinct irradiation regimes, stress confinement and thermal confinement.

The pulse duration of 150 ps is short relative to the characteristic thermal diffusion time across the absorption depth, $\tau_{\mathrm{th}} \sim 10$ ns, but longer than the time of mechanical equilibration of the absorbing volume, $\tau_s \sim 20$ ps. Thus, the simulations with 150 ps pulses are performed in the regime of thermal confinement but not thermoelastic stress confinement. This regime is also characteristic for UV-MALDI conditions.[11] It has been demonstrated recently by Dreisewerd *et al.*[12] that in the regime of thermal confinement the amount of energy deposited by the laser pulse rather than the pulse duration determines the desorption/ablation process. Therefore, even though the pulse duration of 150 ps is an order of magnitude shorter than the pulses commonly used in MALDI, a qualitative comparison between the simulation results and UV-MALDI experimental data is justified.

For the 15 ps laser pulse the condition for stress confinement, $\tau_p \leqslant \tau_s$, is satisfied. In this case a high thermoelastic pressure can be expected to result from the fast energy deposition in the absorption region, leading to an increasing role of photomechanical effects in material removal. The results from this set of simulations can help in understanding of the microscopic mechanisms responsible for energetically efficient ablation in a number of applications, such as IR-

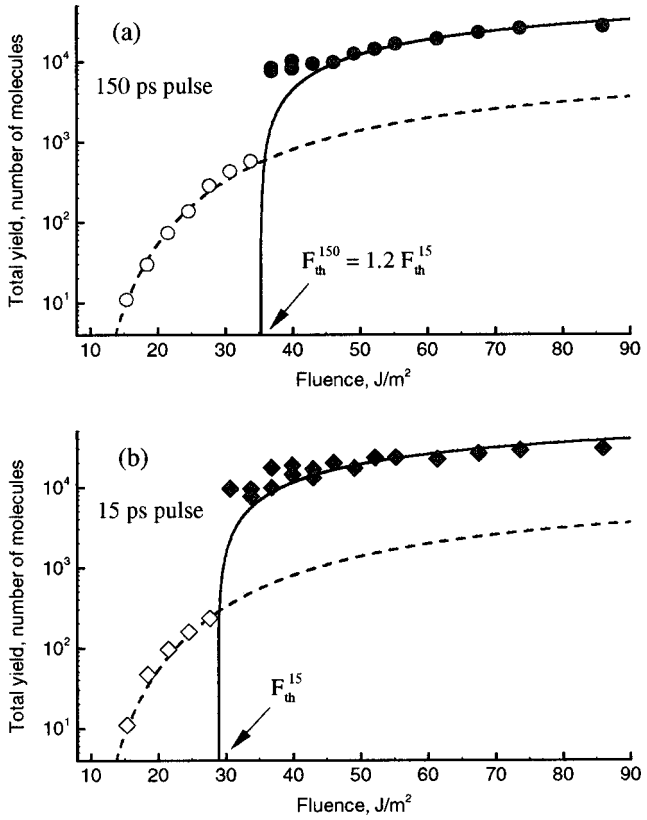

FIG. 3. Total yield as function of laser fluence for simulations with (a) 150 and (b) 15 ps laser pulses. The open and closed symbols show the data points below and above the threshold for ablation. The solid lines represent prediction of the ablation model, Eq. (2), with $E_v^* =$ (a) 0.6 and (b) 0.49 eV. The dashed lines represent fits of the data points below the threshold to the thermal desorption model, Eq. (1). The fits result in the same activation energy, $E_s^* = 0.46$ eV, for both sets of the simulations. A logarithmic scale is used for better presentation of low fluence data.

MALDI and laser surgery, where the regime of stress confinement is realized.[30–36]

III. RESULTS

We now present the results of large-scale MD simulations of laser ablation and damage performed in two different irradiation regimes, stress confinement and thermal confinement. A thorough analysis of the microscopic mechanisms of laser ablation is combined with a systematic investigation of the interrelation between the different parameters of the ablation process accessible for experimental investigation.

A. Fluence dependence of the total yield

The discussions of laser desorption/ablation experimental data are often based on the dependence of the amount of material removed per pulse, i.e., the total yield, on the laser fluence. Thus, we also start the analysis of the simulation results from the yield–fluence dependence that is shown in Fig. 3. A mere visual inspection of the plots shows an apparent similarity in the dependencies for 150 and 15 ps laser pulses. In both cases there are two distinct regimes of molecular ejection separated by a well-defined threshold fluence, F_{th}. The threshold behavior in molecular ejection has been observed in our earlier simulations[6,10,21] and the threshold fluence has been found to separate thermal desorption of molecules from the surface and ablation, a collective ejection in which the processes in the irradiated material at the mesoscopic rather than at the molecular length scale dominate. The results presented in this work are obtained using a larger computational cell and advanced boundary conditions which allows us to perform more detailed quantitative analysis of the yield versus fluence dependencies for two pulse durations.

Let us first consider the ejection at low fluences, or the desorption regime. The lowest fluence at which a noticeable number of molecules desorb from the irradiated surface is 15 J/m^2 for both 150 and 15 ps laser pulses. This fluence can be related to the detection threshold for desorption of neutral matrix molecules in mass spectrometry experiments.[11–13] The energy density deposited at this fluence in the very surface layer of the irradiated sample corresponds to the temperature of 735 K, a value close to the melting point of the model material, $\sim$750 K. As the fluence increases, the yield of desorbed molecules gradually rises and is virtually identical for 150 and 15 ps pulses up to the ablation threshold fluence for the 15 ps pulse, 29 J/m^2. For 150 ps pulses the desorption regime extends up to 35 J/m^2. We find that the dependence of the desorption yield on laser fluence F can be well described by an Arrhenius-type expression,[3,6,11]

$$N = A \exp\left[- \frac{E_s^*}{k_B(T_0 + BF)} \right] \quad \text{for} \quad F < F_{\mathrm{th}}, \tag{1}$$

where N is the number of molecules desorbed during the time of a simulation, E_s^* is an activation energy, A is a pre-exponential or frequency factor, B is a factor that describes the conversion of the deposited energy into an increase of temperature of the surface,[6] T_0 is the initial temperature,[56] and k_B is Boltzmann's constant. As shown in Fig. 3, Eq. (1) provides a good fit of the desorption yield with the same activation energy E_s^* of 0.46 eV for both 150 and 15 ps laser pulses. The pre-exponential factor A divided by the time of the simulation after the end of the laser pulse and the number of molecules at the surface of the computational cell is found to be of the same order as the frequency of molecular vibrations, $\sim 10^{12}$ s^{-1}. The thermal desorption model thus provides an adequate description of the molecular ejection at low laser fluences and the process is not sensitive to pulse duration. A visual inspection of the snapshots from the simulations confirms that mostly monomers are ejected in the desorption regime, Fig. 4.

As can be seen in Fig. 3, the total amount of the ejected material increases at the threshold fluences by more than an order of magnitude. For 150 ps pulses, the increase is from 579 molecules (0.8 nm layer of the original sample) at 34 J/m^2 to 8033 molecules (11.4 nm layer) at 37 J/m^2. For 15 ps pulses, the increase is from 235 molecules (0.3 nm layer of the original sample) at 28 J/m^2 to 9608 molecules (13.6 nm layer) at 31 J/m^2. Clearly, this stepwise transition from ejection of about a monolayer of molecules to a collective ejection, or ablation, of a significant part of the absorbing volume is a reflection of qualitative changes in the ejection mechanism. The thermal desorption model is not valid in the ablation regime and a different analytical description of the

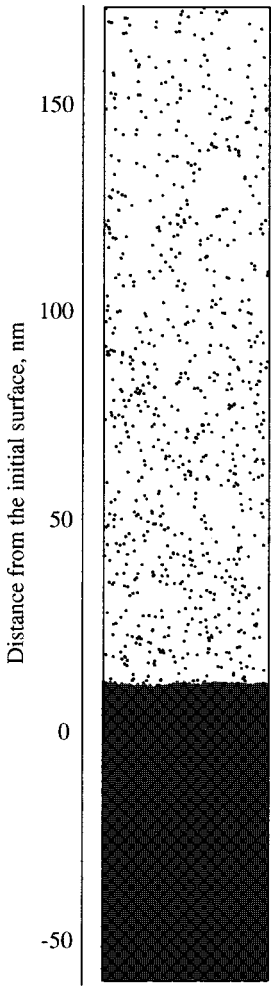

FIG. 4. Typical snapshot from a simulation in the desorption regime. The laser pulse duration is 150 ps and the fluence is 28 J/m^2; the snapshot is made 600 ps after the beginning of the pulse.

yield versus fluence dependence should be used. We find that, for both pulse durations used in the present work, the amount of material ejected in the ablation regime can be relatively well described by a simple model in which the ablation depth follows the laser energy deposition and all material that absorbs an energy density higher than a critical energy density, E_v^*, is ablated.[3,6,24] With an exponential decay of laser intensity given by Beer's law, the total number of molecules ejected per unit surface area is

$$N = n_m L_p \ln\left[\frac{F}{L_p(E_v^* - CT_0)}\right], \quad \text{for } F \geqslant F_{\text{th}}, \tag{2}$$

where n_m is the molecular number density of the material and C is a specific heat capacity of the model material; CT_0 is the thermal energy density prior to laser irradiation. This expression predicts the existence of the threshold fluence $F_{\text{th}} = L_p(E_v^* - CT_0)$ at which the critical energy density E_v^* is reached in the surface layer.

For MALDI, the analytical models for the regimes of thermal desorption and volume ''layer-by-layer'' ejection are discussed by Johnson[3] and by Johnson and Sundqvist[57] and the expressions similar to Eqs. (1) and (2) are used to describe the yield of ejected molecules. The third, pressure pulse, model discussed in Ref. 3 can be related to the simulation results in the regime of stress confinement described in Sec. III B 2.

As shown in Fig. 3, the threshold fluence as well as the value of the critical energy density E_v^* are ~20% higher for irradiation with 150 ps pulses as compared to the values for 15 ps pulses. The ablation yield for 15 ps pulses is consistently higher than the one for 150 ps pulses for all fluences above the threshold fluence. A visual analysis of the snapshots from the simulations[58] given in Sec. III B clearly shows that, although the same analytical equation can be applied to describe the ablation yield in thermal and stress confinement irradiation regimes, the mechanisms responsible for the ablation onset for 150 and 15 ps laser pulses are different. The difference in the ejection mechanisms is reflected in quantitative differences in the threshold fluence and yield versus fluence dependence.

B. Visual pictures and mechanisms of laser ablation and damage

1. Thermal confinement–phase explosion

We start from the analysis of material ejection in the regime of thermal confinement, realized in the simulations with 150 ps laser pulses. Snapshots from a simulation performed at laser fluences of 61 J/m^2, Fig. 5, give a visual picture of the dynamics of laser ablation in this irradiation regime. At ~50 ps from the beginning of the laser pulse irradiated material starts to expand in response to the laser heating. Starting from ~100 ps this expansion is taking on an explosive character leading to the ejection of a significant part (27 nm layer) of the original sample. The snapshot taken at 225 ps shows an onset of a homogeneous decomposition of the expanding plume into a mixture of sublimated molecules and liquid phase matter. This decomposition proceeds through the formation of a foamy transient structure of interconnected liquid clusters and individual molecules, as shown by snapshots at 300 and 375 ps. The foamy transient structure subsequently decomposes into separate clusters, snapshots at 450 and 525 ps, which gradually develop into well-defined spherical liquid droplets, snapshots at 525, 600, and 1000 ps. The process of droplet formation is complete by the end of the simulation, 1000 ps. Longer simulations performed for two-dimensional systems[21] have shown that droplets can shrink somewhat and the number of individual molecules can increase due to the evaporation from the droplets at times that are beyond the end of the simulations discussed in the present work. These changes, however, are relatively minor and the droplets remain a major integral part of the ejected plume.

The picture of the explosive ejection and spontaneous homogeneous decomposition of the ejected material into individual molecules and liquid droplets is consistent with the explosive vaporization mechanism predicted from classical thermodynamics.[7–9,59] As discussed in detail by Kelly and Miotello, short pulse laser irradiation can overheat a bulk part of the absorbing region up to the limit of thermodynamic stability leading to a rapid phase transition of the overheated material into a mixture of gas phase molecules

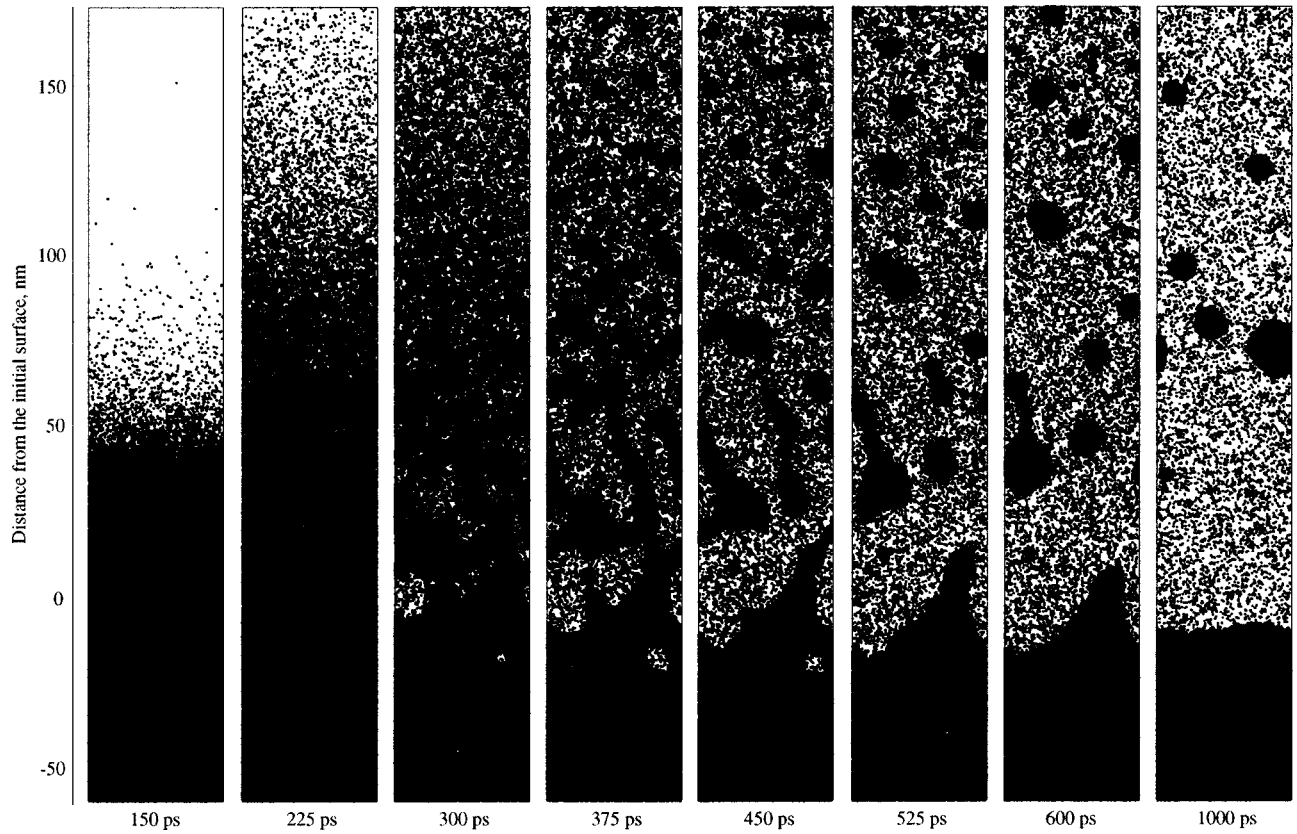

FIG. 5. Snapshots from the MD simulation of laser irradiation of a molecular solid with pulse duration of 150 ps and fluence of 61 J/m^2.

and liquid droplets.[7,8,60] The relative amount of the gas phase molecules is related to the degree of overheating[9] and provides a driving force for the expansion of the ablation plume. In the simulations the fraction of individual molecules in the ejected plume indeed decreases from 25% at the maximum fluence studied, 86 J/m^2, to 9% at the threshold for ablation, 37 J/m^2. In the simulation performed close to the ablation threshold and illustrated by snapshots shown in Fig. 6, the expansion of a relatively small gas phase fraction of the plume barely provides the momentum for ejection of one cluster that is moving out from the sample with a velocity of 165 m/s. The ablation threshold in the regime of thermal confinement is defined, therefore, by the overheating of the absorbing volume up to the point at which the explosive nucleation of the gas phase is sufficient for the ejection of liquid droplets.

The ejection of liquid droplets observed in the simulations can be directly related to the recent results from trapping plate experiments by Handschuh *et al.*[17] performed under UV-MALDI conditions. The fluence dependence of the ejection of small submicron sized clusters observed in Ref. 17, namely, no cluster ejection below the ablation threshold, the appearance of clusters right above the threshold and decreased cluster ejection at higher laser fluences, is consistent with the simulation results. Similar threshold behavior for droplet ejection, albeit for a metal target, has been observed in scattering measurements by Song and Xu.[19] For polymer ablation, the generation of particulates of different sizes has been observed by Heitz and Dickinson.[20] Indirect evidence of the ejection of molecular clusters has been obtained in recent postionization time-of-flight mass spectrometry experiments by Hankin and John.[18] A possible role of cluster ejection for the ionization processes in MALDI has been recently discussed by Karas *et al.*[61]

One important consequence of the phase explosion is the fast cooling of the ejected plume. As a measure of temperature in the plume we use the radial (parallel to the surface) velocity components of the ejected molecules, which do not contain a contribution from the flow velocity of the plume. As found in earlier simulations,[43,44] the distributions of radial velocities fit well to a Maxwell–Boltzmann distribution, suggesting the association of the spread in the radial velocities with the thermal motion in the plume.

The average temperature, calculated from the radial velocities of molecules in a top part of the irradiated sample, is shown in Fig. 7(a) for the simulations illustrated in Figs. 5 and 6. The temperature plots show a nearly linear increase of the temperature during the laser pulse and a fast cooling during the phase explosion. At the higher fluence a more violent explosion leads to the faster temperature drop and, by 500 ps, the average temperature becomes even lower than for irradiation with the lower fluence that is close to the ablation threshold. This can be explained by the fact that in the simulation with 39 J/m^2 only an 11.4 nm layer of the original sample is ejected and $\sim$37% of the particles over which the average has been made still remain in the target. The evaporation from the surface and thermal conduction into the bulk of the sample provide much slower cooling compared to the phase explosion and subsequent evaporation from the ejected droplets. Temperature profiles similar to the ones shown in

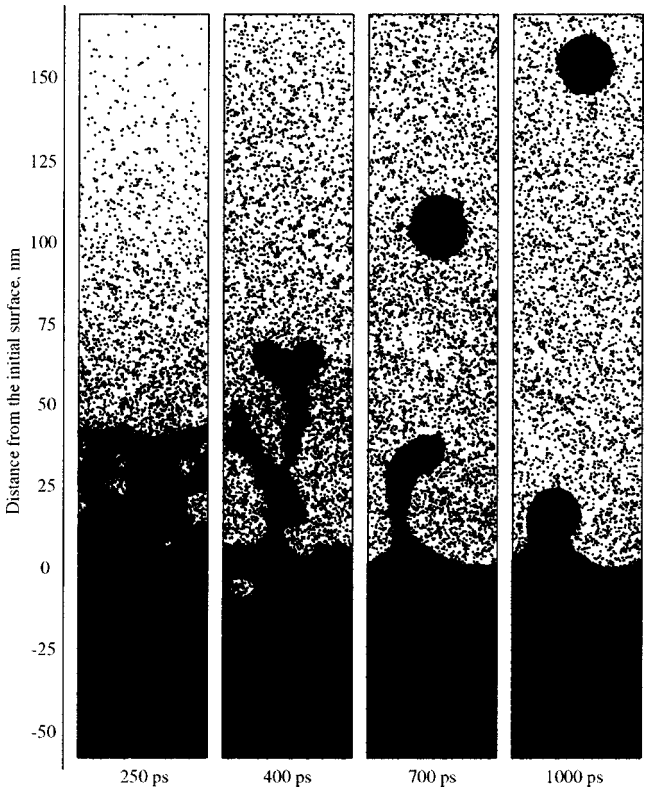

FIG. 6. Snapshots from the MD simulation of laser irradiation of a molecular solid with pulse duration of 150 ps and fluence of 39 J/m^2.

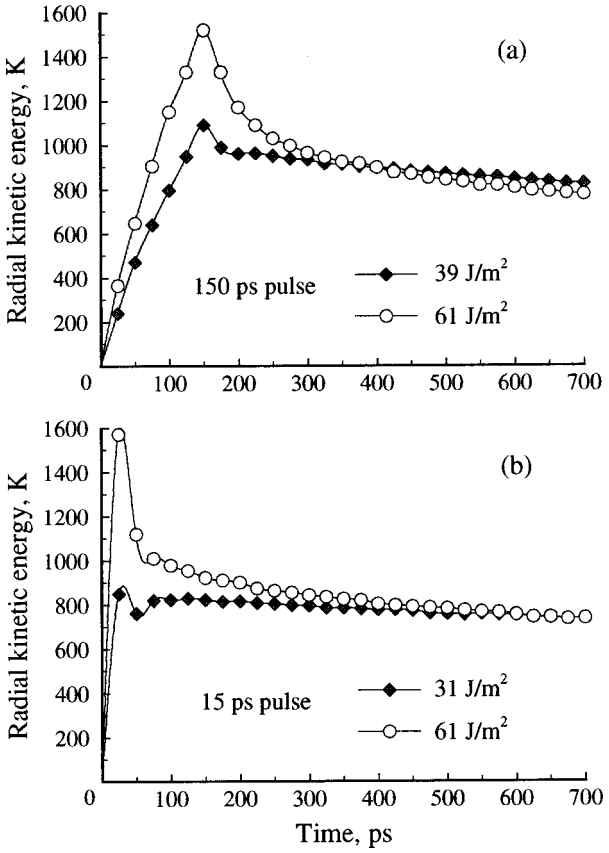

FIG. 7. Averaged radial kinetic energy (in temperature units) of the molecules that belong to the top 18 nm layer of the original sample for simulations with (a) 150 and (b) 15 ps laser pulses.

Fig. 7(a) have been previously observed in two-dimensional MD simulations of laser ablation[21] and ion bombardment.[62] In both cases the fast cooling is attributed to the phase explosion of the overheated material. The fast cooling and the short time in the overheated state could be important factors responsible for survivability of large analyte molecules in MALDI.[1,2,21]

2. Stress confinement–photomechanical effects

A lower threshold fluence observed for irradiation with 15 compared with 150 ps pulses, Fig. 3, is indicative of the difference in the physical processes responsible for the onset of ablation. Indeed, a visual inspection of the snapshots from the simulations performed with 15 ps laser pulses reveals that the mechanism of material ejection at laser fluences close to the ablation threshold is rather different from the phase explosion described above. Figure 8 shows snapshots from a simulation performed at laser fluence of 31 J/m^2, close to the threshold for the ablation onset. At ~75 ps from the beginning of the laser pulse a few voids are nucleated at a certain depth under the irradiated surface. The snapshots taken at 100, 200, and 500 ps show a fast growth of one of the voids that eventually leads to the separation of a large surface layer from the bulk of the sample, as shown by the snapshot at 1000 ps. The number of molecules in the ejected layer corresponds to the 16 nm layer of the original sample. The average temperature of the layer is 726 K, a value below the melting temperature of the model material.

For simulations with 15 ps pulses the void nucleation and growth are the dominant processes of laser ablation and damage in a relatively wide range of fluences, from ~25 up to ~35 J/m^2. At lower laser fluences the initial void nucleation and growth do not lead to the material ejection and are followed by the collapse of the voids, as illustrated by snapshots in Fig. 9. Just below the ablation threshold we observe the formation of bigger voids that do not disappear with time, leading to a permanent damage to the irradiated sample. An accumulation of the laser-induced damage could lead to the material ejection in a multipulse irradiation re-

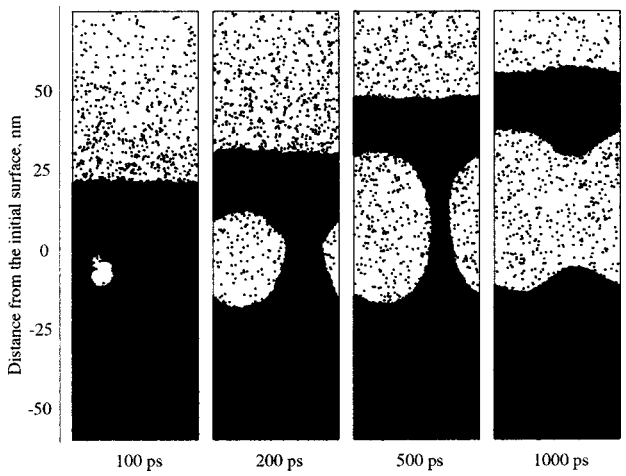

FIG. 8. Snapshots from the MD simulation of laser irradiation of a molecular solid with pulse duration of 15 ps and fluence of 31 J/m^2.

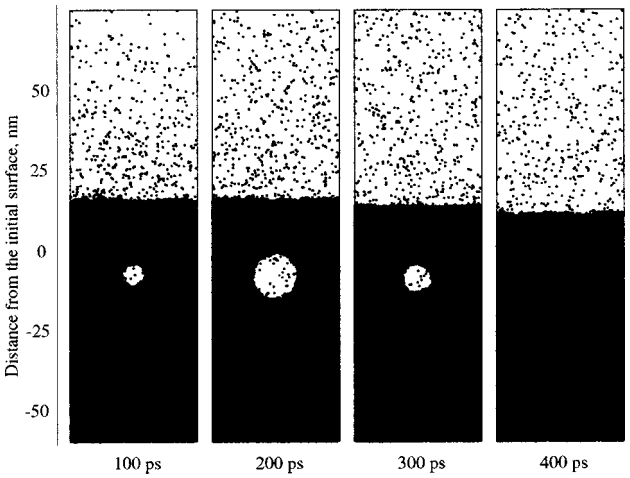

FIG. 9. Snapshots from the MD simulation of laser irradiation of a molecular solid with pulse duration of 15 ps and fluence of 28 J/m^2.

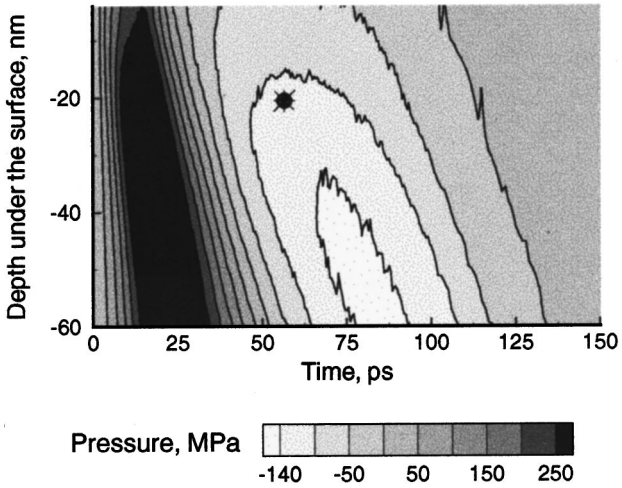

FIG. 10. Pressure contour plot for simulation with a 15 ps laser pulse at laser fluence of 28 J/m^2 illustrated by Fig. 9. The depth and time of the void nucleation are marked by (✸).

gime or in the case of free electron laser irradiation by a macropulse consisting of a series of micropulses.[33]

In order to understand the physical processes that are driving the void nucleation and growth, the temperature and pressure developments in the irradiated sample are considered. The radial temperature plot given in Fig. 7(b) for the simulation performed at a laser fluence just above the threshold for the ablation and illustrated by Fig. 8 shows that the average temperature of the surface layer only slightly exceeds the melting temperature and then slowly cools down. There are no overheating and fast temperature drop that is characteristic of the phase explosion. Moreover, the average temperature of the material at the depths where the voids are nucleated and growing in simulations illustrated by Figs. 8 and 9 is below the melting point of the material. This is indicative of a nonthermal character of the void nucleation and growth.

The analysis of the processes induced by irradiation with 15 ps laser pulses has revealed that the mechanism of void formation and disintegration of the surface layer, illustrated in Figs. 8 and 9, has a mechanical character. The condition of stress confinement, realized in simulations with 15 ps laser pulses, results in the buildup of a high pressure within the absorbing region during the laser pulse. The pressure buildup can be seen in Fig. 10, where the spatial and time development of the local hydrostatic pressure in the irradiated sample is shown in the form of a contour plot for the simulation illustrated by Fig. 9. Interaction of the laser-induced pressure with the free surface leads to the development of the tensile component of the pressure wave propagating from the irradiated surface. The tensile stresses can exceed the dynamic tensile strength of the material[63,64] at a certain depth under the surface and can cause mechanical fracture or spallation. In the simulations the mechanical fracture of the model molecular solid proceeds in the form of void nucleation and growth, Figs. 8 and 9. A similar mechanism of the mechanical fracture has been proposed theoretically[63] and observed in molecular dynamic simulations[65] for the spallation at high strain rates.

The amount of material ejected in laser ablation driven by the relaxation of the laser-induced pressure is defined by the depth at which the spallation occurs. The factors that control the depth of the photomechanical damage and spallation are discussed below. Both the results of analytical calculations[27,30,34] and observations from the simulations for laser fluences below the threshold for void nucleation predict that the maximum tensile stresses are reached at approximately one penetration depth beneath the surface. The void nucleation, however, is consistently observed much closer to the surface, Figs. 8 and 9. In order to understand this discrepancy, the strong temperature dependence of the capability of material to support tensile stresses must be taken into account. The tensile strength of the material heated by laser irradiation decreases significantly as the temperature approaches the melting temperature. The depth of the photomechanical damage is determined therefore not only by the amplitude of the tensile component of the pressure wave, that is increasing from zero at the surface up to a maximum value at the penetration depth, but also by a strong temperature gradient produced within a surface region by laser irradiation. This can be illustrated by the simulation shown Fig. 9, for which the depth and time of the void nucleation are marked in the pressure plot in Fig. 10. The void nucleation coincides with the time when the tensile component of the pressure wave is reaching -120 MPa at a depth of ~ 20 nm under the surface. This depth is less than half the laser penetration depth and the region of the void nucleation is significantly weakened by the laser heating. Although a higher tensile pressure, up to -150 MPa, is reached deeper in the sample, Fig. 10, it does not cause mechanical fracture of the colder and stronger region.

For higher laser fluences the void nucleation can proceed not only at the depth defined by the balance between the increasing tensile stresses and the thermal softening, but over a larger volume in the surface region. This effect can be illustrated by snapshots from the simulation at laser fluence of 34 J/m^2 shown in Fig. 11. In this simulation several voids are developing within the surface region during ~ 200 ps

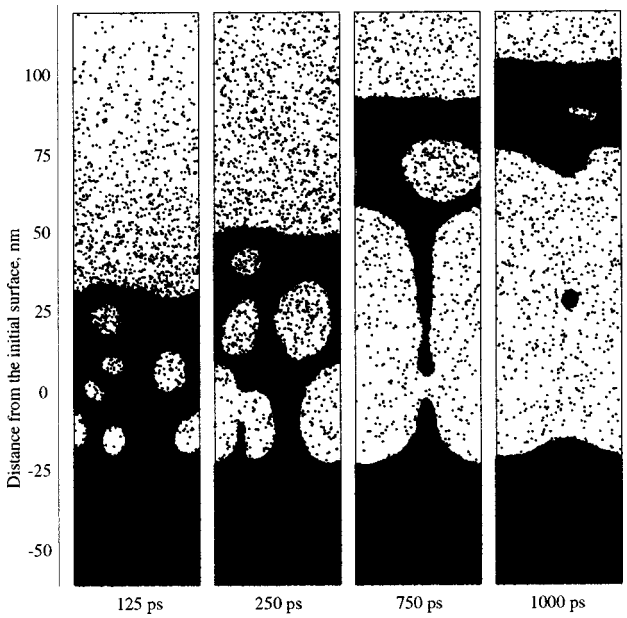

FIG. 11. Snapshots from the MD simulation of laser irradiation of a molecular solid with pulse duration of 15 ps and fluence of 34 J/m^2.

following the laser irradiation. At later times the deeper voids continue to grow, coalesce, and, at 700 ps, a large surface layer is separated from the sample. The number of molecules in the ejected layer corresponds to the 23 nm layer of the original sample, and the average temperature of the layer is 757 K. The mechanical stability of the surface region subjected to the void nucleation is strongly affected by the laser heating and the analytical prediction on the formation of multiple spallation planes in the absorption region[34] cannot be directly applied for a quantitative description of the simulation results.

As discussed above, the void nucleation and growth shown in Figs. 8, 9, and 11 are caused by the tensile stresses induced near the irradiated surface in the regime of stress confinement. In the simulations performed for the same laser fluences but with 150 ps, when the same amount of energy is deposited over a 10 times longer period of time, there is no void formation or cluster ejection. Also, the void formation has nothing to do with nucleation and growth of vapor bubbles in the course of heterogeneous (normal) boiling. Moreover, estimates of the kinetics of normal boiling given in a recent paper by Kelly and Miotello clearly demonstrate the irrelevance of this process to short pulse laser ablation.[8]

The ablation process at higher laser fluences, when material ejection is driven by a combination of the strong pressure gradient formed due to the stress confinement and the phase explosion due to the overheating, is considered next. The dynamics of laser ablation in this irradiation regime is illustrated in Fig. 12 for a simulation performed at laser fluences of 61 J/m^2. This fluence is the same as that in the simulation performed with the longer, 150 ps, laser pulse that is illustrated by Fig. 5. At first the visual pictures of material ejection shown in Figs. 5 and 12 look similar. More detailed analysis, however, reveals several important differences.

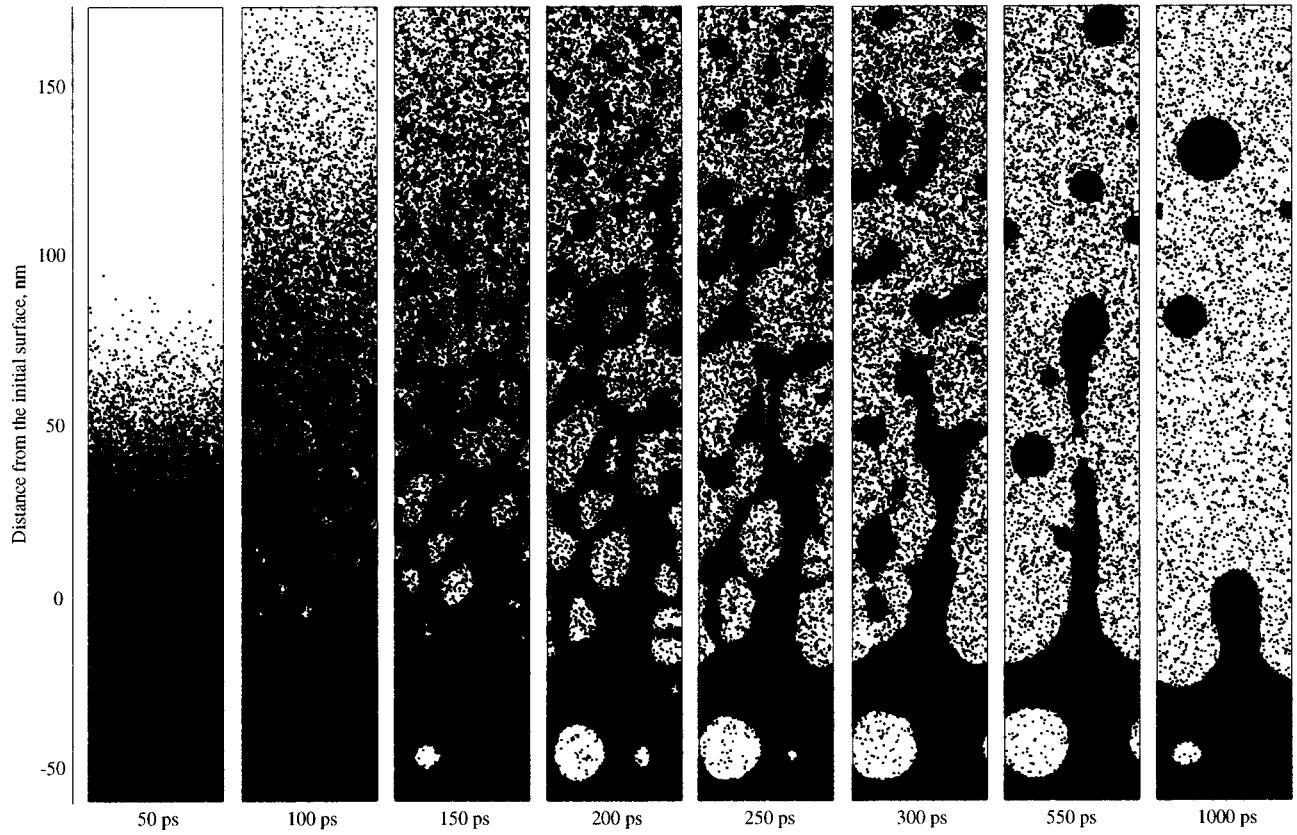

FIG. 12. Snapshots from the MD simulation of laser irradiation of a molecular solid with pulse duration of 15 ps and fluence of 61 J/m^2.

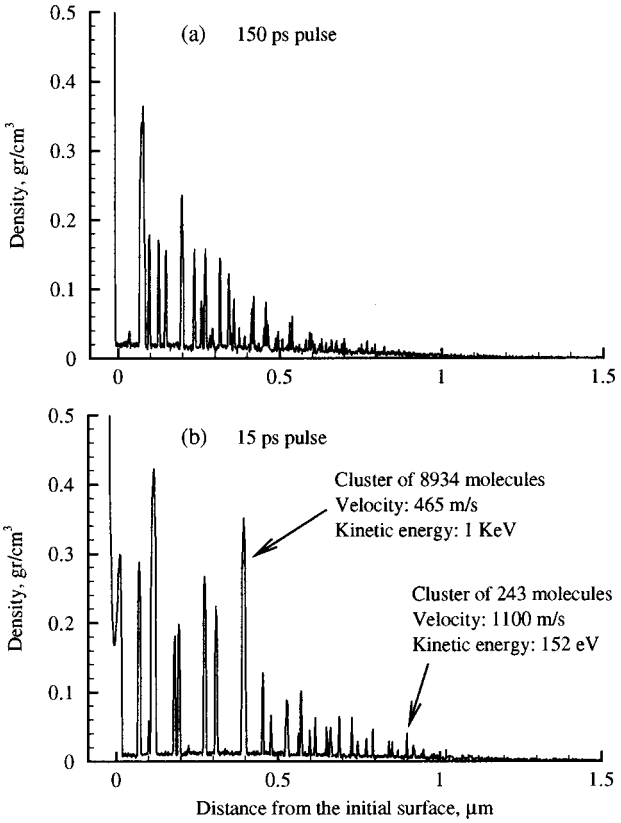

FIG. 13. Density of the ejected plume as a function of the distance from the initial surface for simulations with (a) 150 and (b) 15 ps laser pulses and fluence of 61 J/m^2 shown for 850 ps after the end of the laser pulses. Snapshots from the simulations are shown in Figs. 5 and 12.

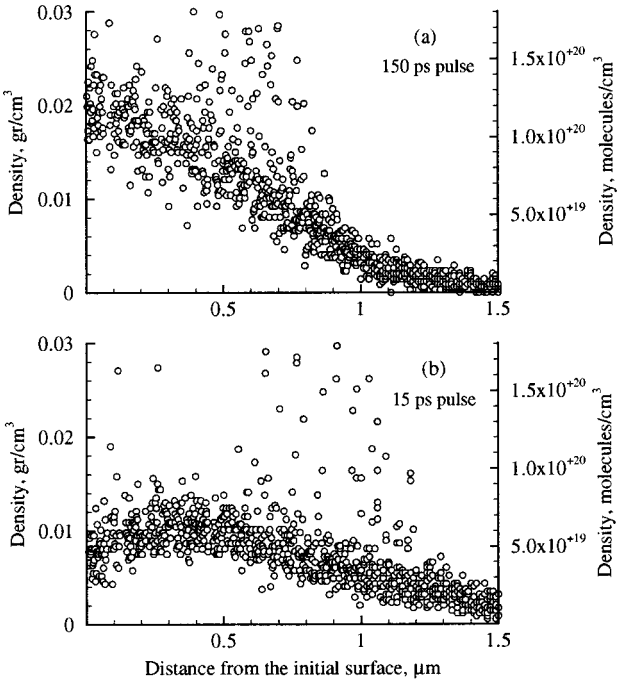

FIG. 14. Same as in Fig. 13. The region of low density that shows the density of the gas-phase molecules in the ejected plume is presented. Each point results from averaging over a 1.5 nm span along the normal to the surface.

First, the total amount of ejected material is ~17% larger in the simulation with a 15 ps pulse as compared to the one with a 150 ps pulse. Actually, as discussed in Sec. III A, the total yield of ejected molecules is consistently higher for 15 ps pulses in the whole range of fluences above the ablation threshold.

Second, the void formation, observed in the stress confinement regime at laser fluences close to the ablation threshold, Figs. 8, 9, and 11, is also present at higher fluences. In Fig. 12 a transient void forms at the depth of ~50 nm, below the surface layer ejected in the course of ablation. The void formation is not observed in the thermal confinement regime at any laser fluences investigated.

Third, larger and more numerous clusters are ejected in the simulation shown in Fig. 12 as compared to the one shown in Fig. 5. The cluster ejection can be seen from Fig. 13, where the number of peaks and their heights reflect the number of ejected clusters and their sizes, respectively. As will be shown in Sec. III C, these are the clusters that are mainly responsible for the increase in the total yield as we go from the regime of thermal confinement to the regime of stress confinement, whereas the yield of monomers is nearly identical in the two ejection regimes.

Fourth, a more prompt disintegration and ejection observed in the regime of stress confinement, Fig. 12, lead to the ejection of clusters with significantly higher velocities in the direction normal to the surface, as compared to the regime of thermal confinement. The difference in the velocities of the clusters can be seen from the difference in the spread in the peak positions in Figs. 13(a) and 13(b). By 850 ps after the end of the laser pulse some of the small clusters ejected in the stress confinement regime have traveled a distance of nearly 1 μm from the initial surface as shown in Fig. 13(b) for a cluster composed of 243 molecules and moving with a velocity of 1100 m/s. A large cluster composed of 8934 molecules and moving with a velocity of 465 m/s is also marked in the Fig. 13(b). The ejection of such energetic clusters is not observed in the regime of thermal confinement, Fig. 13(a).

Fifth, the density distribution of the gas-phase molecules that shows up as a background level in the density profiles in Fig. 13 is different in the simulations illustrated by Figs. 5 and 12. Qualitatively, the difference is apparent from a visual inspection of the snapshots taken at the end of the simulations. A significantly higher density of the cloud of individual molecules is observed in Fig. 5 than in Fig. 12. To perform a quantitative comparison, an expanded view of the low-density region of Fig. 13 is shown in Fig. 14. The density of individual molecules right above the surface observed for the simulation performed with a 15 ps pulse, Fig. 14(b), is less than half the density observed for the simulation performed with a 150 ps pulse, Fig. 14(a). At the same time, a significantly higher density is observed in the simulation with a 15 ps pulse further from the surfaces, at distances of 1 μm and more. Apparently, in the case of irradiation with 15 ps pulses, the cloud of individual molecules travels faster and disperses more during the same time after the end of the laser pulse. This observation can be attributed to the stronger pressure gradient that results from irradiation under the condition of stress confinement and provides higher initial accel-

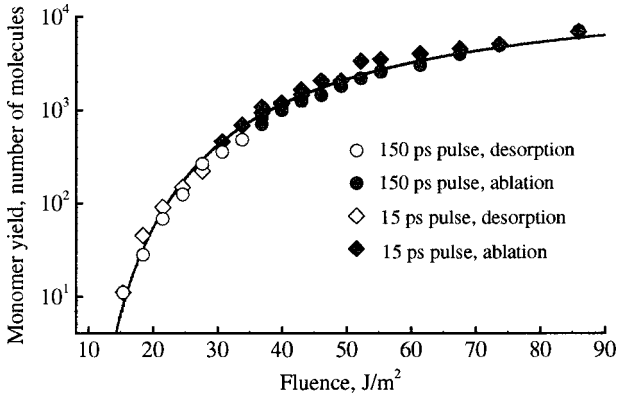

FIG. 15. Yield of monomers as a function of laser fluence. The circles and diamonds represent the data points for 150 and 15 ps laser pulses, respectively. The open and closed symbols show the data points below and above the threshold for ablation. The line shows the prediction of the thermal desorption model, Eq. (1), with activation energy of 0.52 eV.

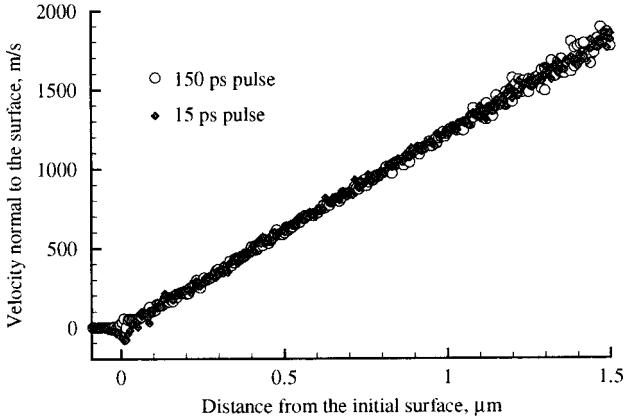

FIG. 16. Flow velocity in the ejected plume as a function of the distance from the initial surface for simulations with 150 ps and 15 ps laser pulses and fluence of 61 J/m^2 shown for 850 ps after the end of the laser pulses. Each point results from averaging over a 6 nm span along the normal to the surface. Snapshots from the simulations are shown in Figs. 5 and 12.

eration of the ejected material. A more detailed comparative analysis of the plume composition and the velocities of ejected species in the stress and thermal confinement regimes is given in Sec. III C.

C. Parameters of the ejected plume

In mass spectrometric applications of laser ablation the characteristics of the ejected plume are the relevant parameters that define the resolution and quality of mass spectra. The experimental measurements in these applications are often limited to counting the ejected ions or postionized molecules[11–13] and deriving their initial velocities.[14,15,66] It is difficult to provide a reliable interpretation of these data in terms of the physical mechanisms leading to the material ejection and processes occurring at the initial stage of dense plume expansion. Here in Sec. III C we take advantage of the comprehensive picture of the laser ablation process resulting from the molecular-level simulations and perform a comparison analysis of the plume composition, velocity, and angular distributions of the ejected particles in the regimes of thermal and stress confinement.

The visual pictures of the ejected plume given in Sec. III B show clearly that large molecular clusters constitute a major portion of the ejected plume in the ablation regime and that the composition of the ejected plume has a strong dependence on laser fluence and pulse duration. To perform a quantitative analysis of the plume composition we compare the fluence dependencies of the total yield, Fig. 3, with the yield of monomers, a quantity that is presumably proportional to the yield of ions or postionized neutral molecules measured in mass spectrometry experiments. The fluence dependence of the yield of monomers given in Fig. 15 is in drastic contrast to the total yield curves, Fig. 3. First, although the total number of ejected molecules is increasing at the ablation threshold by more than an order of magnitude, this sharp increase is imperceptible in the fluence dependence of the monomer yield. Evidently, it is the onset of the ejection of clusters that is responsible for the jump in the total yield at the threshold fluence.[6,10] Second, the yields of monomers are nearly identical in the regimes of thermal and stress confinement. As shown in Fig. 15, Eq. (1) provides a good description of the monomer yield for both 150 and 15 ps laser pulses with the same value of activation energy, $E_s^* = 0.52$ eV. Despite the seemingly good fit of the monomer yield, the thermal desorption model leading to Eq. (1) does not give a correct description of the ejection mechanism at high fluences, where collective ejection or ablation occurs. Therefore, an interpretation of the physical mechanisms of laser ablation[11,13] and, in particular, a discussion of the role of the laser pulse duration[12,33,67] should not be based solely on the mass spectrometry data on the yield of ejected ions, but should be complemented by measurements of other characteristics.

As has been noted in Sec. III B, the difference in the ejection mechanisms in the regimes of thermal and stress confinement is reflected in the sizes and velocities of the ejected clusters. Although the limited size of the computational cell restricts our ability to perform a reliable quantitative analysis of the size distribution of the ejected clusters, qualitatively we can conclude that larger and more numerous clusters are ejected in simulations with 15 ps pulses as compared to 150 ps pulses. To analyze the velocities of the ejected clusters, the density profiles shown in Fig. 13 can be related to the distributions of flow velocities in the ejected plume, Fig. 16. By 850 ps after the end of the laser pulses the velocities for the two pulse durations have acquired identical linear dependencies on the distance from the surface that is characteristic for the free expansion model.[68] A small dip into the negative velocities at the position of the original surface observed in Fig. 16 for the simulation with a 15 ps pulse can be attributed to active hydrodynamic motion during the relaxation of the transient topographical features formed in the surface region of the irradiated sample, Fig. 12. The comparison of the density and velocity profiles given in Figs. 13 and 16 shows that there is no correlation between the cluster positions (peaks in Fig. 13) and the flow velocities in the expanding plume. The clusters of different sizes are entrained into the expanding plume and are moving along with the individual molecules with the same velocities. This

effect of entrainment of molecular clusters can be related to the entrainment of large biomolecules into the plume of smaller matrix molecules in MALDI that has been observed experimentally[14,66,69,70] and in MD simulations.[44] The threshold fluence for the detection of analyte molecules in MALDI,[17,21,44] nonvolatile photoproducts,[71] or dopants[72] in laser ablation of molecular films can be related in this case to the threshold fluence for the onset of the collective material ejection or ablation.

Experimentally, the properties of the ejected plume are often probed by measuring the velocity distributions of the ejected molecules.[14,15,69] In particular, the velocity distributions of neutral molecules measured by laser postionization mass spectrometry techniques[14,15] can be related to the calculated velocity distributions of ejected individual molecules. Figures 17 and 18 show velocity distributions that are typical representatives of the distributions observed for desorption, ablation in the regime of stress confinement, and ablation in the regime of thermal confinement. For all simulations the distributions of radial (parallel to the surface) velocity components can be well described by a Maxwell–Boltzmann distribution, Fig. 17. Although a more than two times higher fluence is used in the simulations of ablation compared to the desorption, the temperatures resulting from the fits to a Maxwell–Boltzmann distribution exhibit much smaller variation. This observation can be explained by the fast cooling of the ejected plume in the course of explosive decomposition and expansion, Fig. 7. A somewhat lower temperature of the plume in the regime of stress confinement, Fig. 17(b), as compared to in thermal confinement, Fig. 17(c), is related to more rapid material disintegration and ejection observed under the conditions of stress confinement.

In contrast to the radial velocities, the distributions of axial (normal to the surface) velocity components exhibit a significantly stronger dependence on the irradiation conditions. In the desorption regime, Fig. 18(a), the distribution can be relatively well described by a shifted Maxwell–Boltzmann distribution with the same temperature of 525 K that results from the fit of the radial velocity distribution in Fig. 17(a). The equilibration of the ejected molecules and the appearance of the molecules with negative velocities in the desorption regime can be attributed to the gas-phase collisions[73] during the intensive evaporation from the irradiated surface, Fig. 4.

In the ablation regime, Figs. 18(b) and 18(c), much broader highly asymmetric velocity distributions with high-velocity tails that extend beyond 2000 m/s are observed. Similar asymmetric velocity distributions have been observed experimentally for laser ablation of molecular solids[14,15] and in earlier two-dimensional MD simulations.[43] Simulation results suggest that collective material ejection in the ablation regime provides an initial broad distribution of the flow velocities in the ablation plume. Subsequent collisions in the expanding plume result in redistribution of the energy and momentum in the axial direction,[21] leading to additional acceleration of the molecules in the front of the plume and formation of the high-velocity tail in the axial velocity distributions. The velocity distributions can be roughly described by a modified Maxwell–Boltzmann distribution that has been proposed in Refs. 43 and 44 in order to account for a range of flow velocities in the ejected plume. The temperatures that result from the fits of the radial velocity distributions to a Maxwell–Boltzmann distribution, Figs. 17(b) and 17(c), are used to describe the axial velocity distributions as well, Figs. 18(b) and 18(c). The spread of the

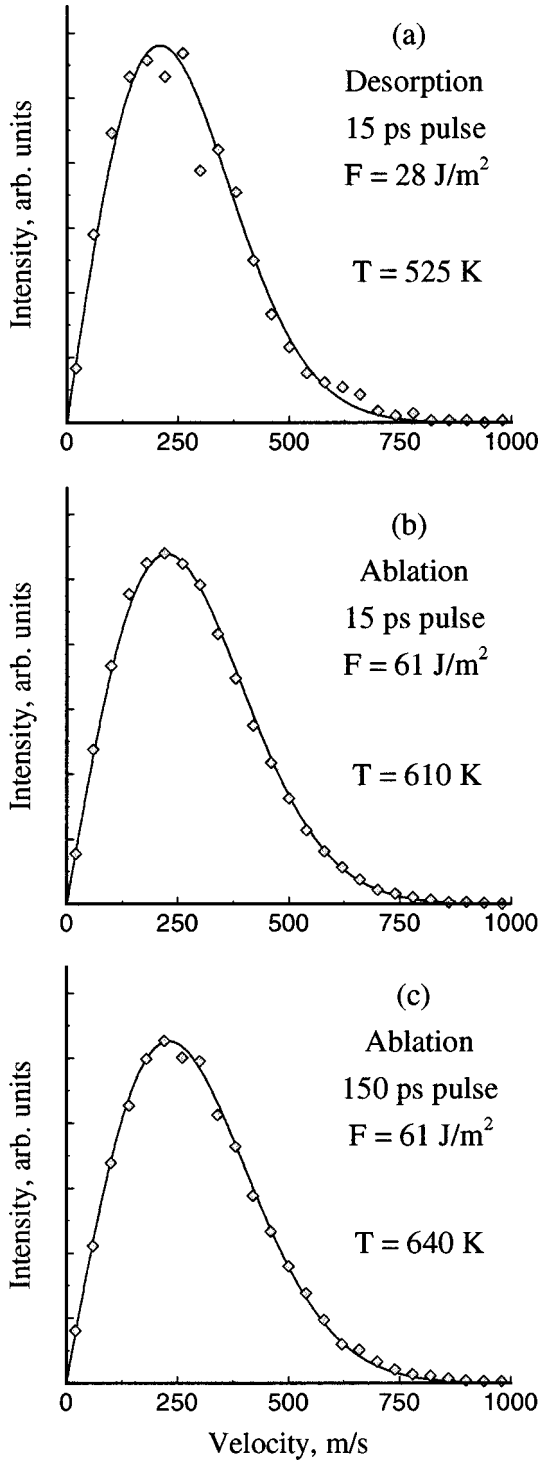

FIG. 17. Radial velocity distributions of ejected monomers for simulations with (a), (b) 15 and (c) 150 ps laser pulses and fluences of (a) 28 and (b), (c) 61 J/m^2. The symbols are data from the simulations and the lines show the Maxwell–Boltzmann distribution for temperatures of (a) 525, (b) 610, and (c) 640 K.

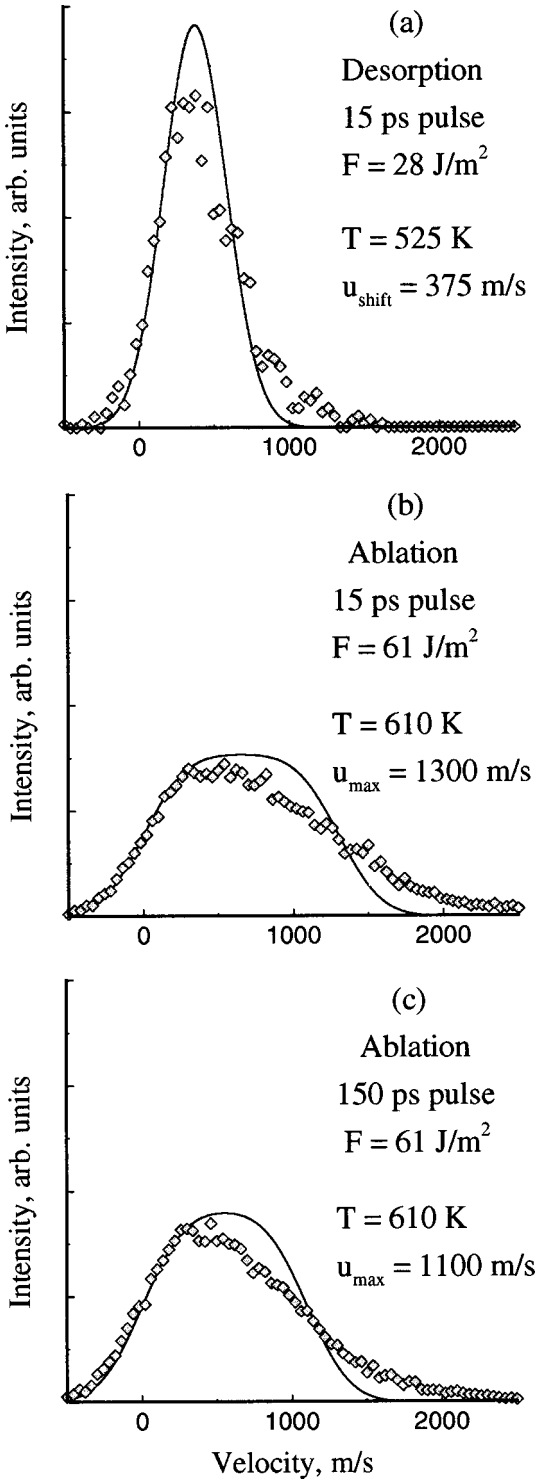

FIG. 18. Axial velocity distributions of ejected monomers for simulations with (a), (b) 15 and (c) 150 ps laser pulses and fluences of (a) 28 and (b), (c) 61 J/m^2. The symbols are data from the simulations. The lines show (a) the shifted Maxwell–Boltzmann distribution for a temperature of 525 K and a flow velocity of 375 m/s; (b), (c) the Maxwell–Boltzmann distribution with a range of stream velocities (see Refs. 43 and 44) for temperatures of (b) 610 and (c) 640 K and maximum flow velocities of (b) 1300 and (c) 1100 m/s.

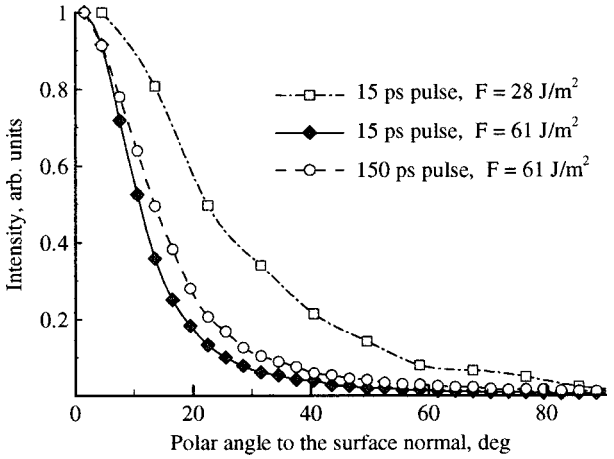

FIG. 19. Angular distributions of ejected monomers for simulations with 15 and 150 ps laser pulses and fluences of 28 and 61 J/m^2.

velocities in the direction normal to the surface is mainly defined by the range of flow velocities in the ejected plume and only to a lesser extent by the thermal motion. A comparison between the axial velocity distributions shown in Figs. 18(b) and 18(c) demonstrates that a broader distribution and a bigger fraction of high-velocity molecules are characteristic for the plume ejected in the stress confinement regime, Fig. 18(b). These differences can be related to a wider dispersion in the positions of ejected clusters, Fig. 13, and more extended density profiles for the gas-phase molecules, Fig. 14, observed in simulations with 15 ps pulses compared to the simulations with 150 ps pulses. Quantitatively, a broader velocity distribution in the regime of stress confinement is reflected in a higher maximum flow velocity, $u_{\max}$, that results from the fit of the data points to the modified Maxwell–Boltzmann distribution, Figs. 18(b) and 18(c). Note that the modified Maxwell–Boltzmann distribution on a range of flow velocities provides only a rough description of the simulation data and the extended high-velocity tails of the distributions cannot be adequately described by any existing analytic distribution.

The angular distributions of the ejected molecules are given in Fig. 19 for the same three simulations for which velocity distributions are discussed above. In the desorption regime, $F=28$ J/m^2, moderate forward peaking is observed that can be attributed to the gas-phase collisions of desorbed molecules leading to Knudsen layer formation.[74] Quantitatively, the angular distributions are commonly described by a $\cos^p(\theta)$ function for small polar angles to the surface normal, θ. For the simulation at $F=28$ J/m^2, where intense desorption leads to the ejection of about one monolayer of molecules, fitting to this form for angles $\theta<20°$ gives $\cos^9(\theta)$ that is consistent with theoretical considerations.[74] In the ablation regime much stronger forward peaking is observed, with fits giving $\cos^{25}(\theta)$ and $\cos^{36}(\theta)$ for the simulations performed in the thermal and stress confinement regimes, respectively. The stronger focusing of ejected molecules toward the surface normal in the stress confinement regime is related to the broader distribution of the axial velocities in Fig. 18(b). Experimentally, strong forward peaking of ejected molecules is typically observed in laser ablation of molecular solids.[15,69,70]

Although good fits of the radial velocity distributions to a Maxwell–Boltzmann distribution shown in Fig. 17 imply at least partial equilibration in the ejection plume, a spatially

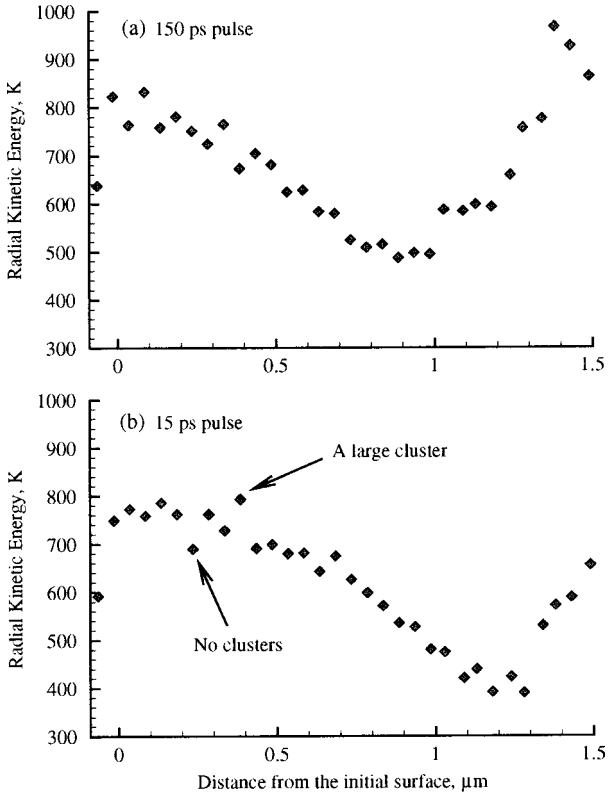

FIG. 20. Radial kinetic energy (in temperature units) of the ejected plume as function of the distance from the initial surface for simulations with 150 and 15 ps laser pulses and fluence of 61 J/m^2 shown for 850 ps after the end of the laser pulses. Each point results from averaging over a 50 nm span along the normal to the surface. Snapshots from the simulations are shown in Figs. 5 and 12.

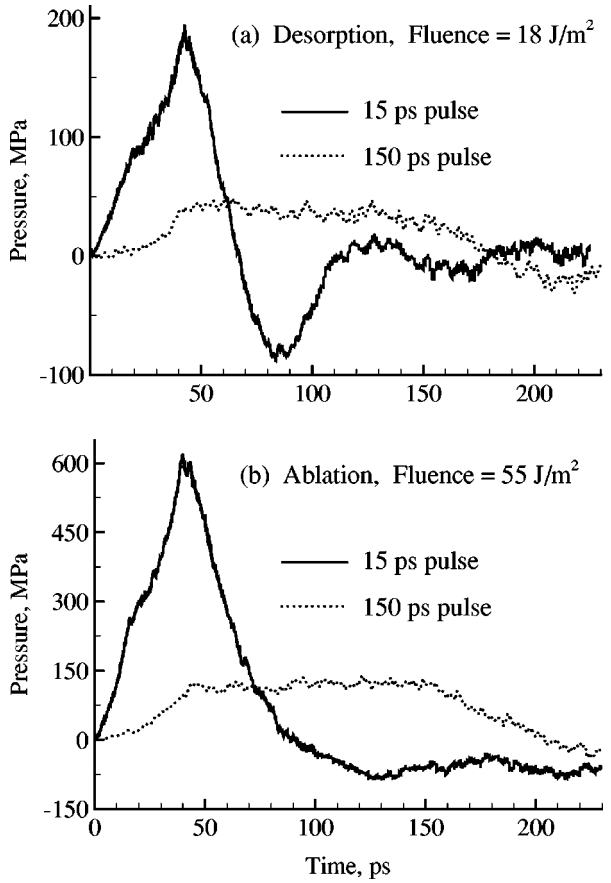

FIG. 21. Temporal pressure profiles at 100 nm below the surface for simulations with 15 and 150 ps laser pulses performed in the (a) desorption and (b) ablation regimes. A computational cell of 180 nm in the direction normal to the surface is used in the simulations.

resolved analysis of the plume in the ablation regime reveals a significant variation of the radial temperature with distance from the irradiated surface. The spatial distributions of the average radial kinetic energy, shown in Fig. 20, suggest that the fast cooling of the ejected material, Fig. 7, proceeds nonuniformly within the plume. Expansion cooling, when the thermal energy is transformed into the kinetic energy of the plume expansion, leads to the decrease of the radial temperature in the flow direction. At distances of 1 μm for a 150 ps pulse and 1.3 μm for a 15 ps pulse, the radial temperature reaches its minimum and starts to increase. This temperature increase that has been also observed in Monte Carlo simulations of a multilayer particle ejection[73] can be attributed to the lack of equilibration in the front part of the expanding plume, where too small densities of ejected molecules are observed, Fig. 14. A significant scattering of the data points in Fig. 20 is due to the difference between the temperatures of gas-phase molecules and clusters in the plume. The clusters are substantially hotter than the gas-phase molecules, reflecting slower cooling by evaporation as compared to fast expansional cooling.

D. Pressure pulse profiles

Time-resolved piezoelectric detection of acoustic waves generated by pulsed laser irradiation has been successfully used in the analysis of the laser-induced processes in a number of organic systems.[16,24,26–28,32,75] Experimental observations indicate that the shape of the pressure wave has a strong dependence on the irradiation conditions and can give useful information on the processes in the absorption region. In this section an analysis of the relations between the character of the molecular ejection in the regimes of thermal and stress confinement and the parameters of the pressure waves is given.

Pressure profiles typical for the desorption and ablation regimes are shown in Fig. 21 for simulations performed with 150 and 15 ps laser pulses. The temporal pressure profiles are recorded at a depth of 100 nm under the initial surface in simulations where the total depth of the computational cell is 180 nm and the dynamic nonreflecting boundary condition is applied at the bottom of the computational cell, as described in Sec. II B. Just as in Figs. 1 and 10, positive pressure corresponds to compression and negative pressure to tensile stresses. For both desorption, Fig. 21(a), and ablation, Fig. 21(b), much stronger pressure waves are initiated in the regime of stress confinement than in the regime of thermal confinement. This observation agrees with experimental observations that a significantly higher pressure builds up in the absorption region[29] and a much stronger acoustic signal is produced[28,75] when the conditions for stress confinement are satisfied.

For simulations with a 15 ps laser pulse, in the stress confinement regime, there is a clear difference in the pressure profiles recorded for desorption and ablation. At low laser fluences, below the threshold for the ablation onset, we observe a characteristic bipolar thermoelastic wave that results from the interaction of the laser-induced compressive pressure with a free surface of the irradiated sample, Fig. 21(a). Certain asymmetry between a stronger compressive component of the wave and a weaker tensile component in Fig. 21(a) can be attributed to the small depth of the pressure recording, 100 nm, that is only two times longer than the laser penetration depth. The direct laser energy absorption at the depth of the recording leads to the pressure increase during the laser pulse[42] and creates a positive background for the symmetric bipolar pressure wave propagating deeper into the sample. As the laser fluence increases above the threshold for the ablation onset, the ratio between the tensile and compressive components of the pressure wave gradually decreases. As a result, a strong unipolar compressive wave is generated in the ablation regime for 15 ps pulses, Fig. 21(b).

The laser fluence dependence of the positive (compressive) and negative (tensile) amplitudes of the pressure waves is plotted in Fig. 22. In simulations with both 150 and 15 ps pulses the peak compressive pressure, Fig. 22(a), increases linearly with fluence as expected for the thermoelastic mechanism of wave generation. The linear dependence extends beyond the ablation threshold, over the whole range of fluences, suggesting that the compressive recoil pressure imparted by the massive material ejection at high fluences does not significantly affect the amplitude of the compressive component of the pressure wave. This observation indicates that generation of thermoelastic stresses and a slower process of material ejection in the ablation regime are separated in time.

The amplitude of the tensile component of the pressure wave exhibits a more complex dependence on laser fluence, Fig. 22(b). At low laser fluences a linear increase of the peak tensile stresses with fluence is observed that corresponds to the gradual increase of the amplitudes of thermoelastic bipolar pressure waves shown in Fig. 21(a). At higher laser fluences, however, the amplitude of the tensile component of the pressure waves saturates and even decreases with the fluence. The transition from linear dependence at low fluences to saturation and decrease at higher fluences has a different character for simulations performed with 150 and 15 ps pulses. For 150 ps pulses a gradual deviation from the linear dependence at laser fluences close to the threshold for the ablation onset and saturation at higher fluences is observed. In contrast, for 15 ps pulses a sharp break in the dependence at the ablation threshold and a significant decrease of the maximum tensile stresses at higher fluences are observed. The last point that follows the linear dependence for 15 ps pulses corresponds to the last simulation that does not lead to massive material ejection, Fig. 9, whereas the first point after the break in the dependence corresponds to the simulation in which separation of a surface layer from the sample is observed, Fig. 8.

The existence of a sharp maximum in the fluence dependence of the tensile pressure amplitude observed in Fig. 22(b) for 15 ps pulses is consistent with the discussion of the photomechanical processes responsible for the ablation onset in the regime of stress confinement given in Sec. III B 2. The material ejection in this case is driven by the relaxation of the laser-induced pressure gradient, the material disintegration leads to the relief of tensile stresses, and the observed maximum amplitude of the tensile stresses corresponds in this case to the dynamic tensile strength of the material. Apparently, the nucleation and growth of localized voids, Fig. 9, do not significantly affect the amplitude of the tensile part of the pressure wave that continues to increase as the wave passes the region of void formation and propagates deeper into the sample, Fig. 10. A significant decrease of the amplitude of the tensile component of the pressure wave as laser fluence increases above the ablation threshold can be explained by the contribution of the following two processes. First, the effect of thermal softening, discussed in Sec. III B 2 can significantly reduce the dynamic tensile strength of the material[63] in the surface region of the sample at higher laser fluences, limiting the capability of the material to support

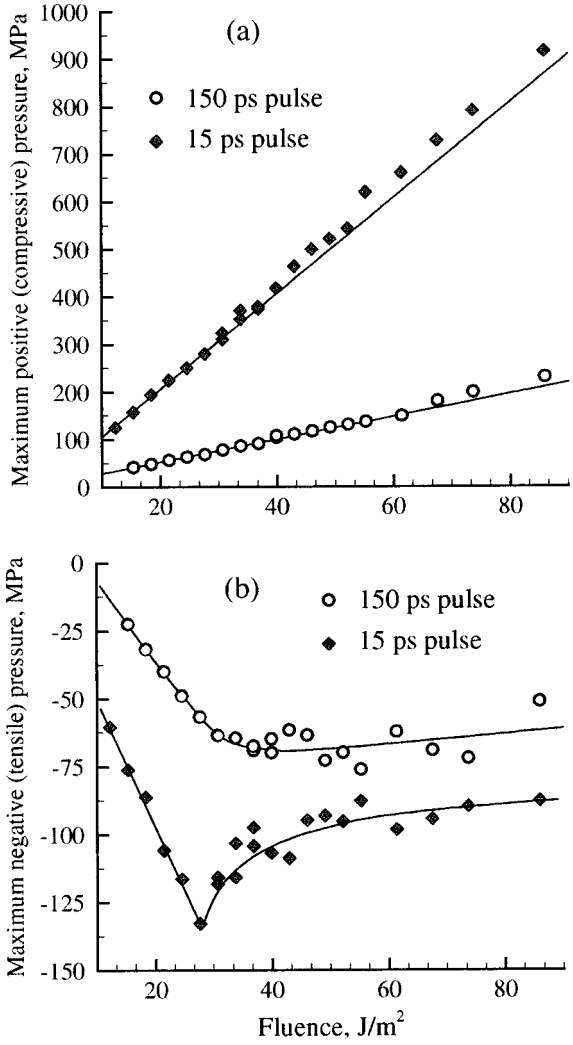

FIG. 22. (a) Positive and (b) negative amplitudes of the pressure wave as a function of laser fluence. The circles and diamonds represent the data points for 150 and 15 ps laser pulses, respectively. Lines in (a) are the linear fits to the data points in the desorption regimes (below 29 J/m^2 for 15 ps pulses and below 35 J/m^2 for 150 ps pulses), and are just guides to the eye in (b).

tensile stresses. Second, the tensile stresses produced by the thermoelastic mechanism can be obscured in the ablation regime by superposition with the compressive recoil pressure from the ejection of the ablation plume.

Experimentally, pressure profiles similar to the ones shown in Figs. 21(a) and 21(b) for 15 ps pulses have been observed for laser irradiation of soft biological tissue below and above the ablation threshold respectively.[75] A fluence dependence of the amplitude of the tensile component of the pressure wave similar to the one shown in Fig. 22(b) for 15 ps pulses has been observed for aqueous media irradiated in the stress confinement regime.[26] Both experimental measurements and the results of the present simulation study suggest that the shape and parameters of the acoustic wave propagating from the absorption region are sensitive to changes in the mechanisms of material ejection and can be used for tuning irradiation parameters to the desired ejection conditions. Simulations allow us to directly relate the characteristics of the pressure waves to the molecular-level picture of laser desorption, ablation, and damage and can help in interpretation of experimental data from photoacoustic measurements.

IV. SUMMARY

The results of large-scale MD simulations performed for two pulse durations and a wide range of laser fluences provide a comprehensive picture of laser ablation and damage in two different irradiation regimes, stress confinement and thermal confinement. We find that the mechanisms responsible for material ejection as well as most of the parameters of the ejection process have a strong dependence on the rate of the laser energy deposition. For longer laser pulses, *in the regime of thermal confinement*, the phase explosion of the overheated material is responsible for the collective material ejection at laser fluences above the ablation threshold. The phase explosion leads to homogeneous decomposition of the expanding plume into a mixture of liquid droplets and gas-phase molecules. This decomposition proceeds through the formation of a transient structure of interconnected liquid clusters and individual molecules and leads to fast cooling of the ejected plume.

For shorter laser pulses, *in the regime of stress confinement*, a lower threshold fluence for the onset of laser ablation and damage is observed. The energetically efficient material ejection is attributed to photomechanical effects driven by the relaxation of high thermoelastic pressure that builds up in the absorption region under the conditions of stress confinement. Laser ablation in this case proceeds through void nucleation and growth which eventually lead to disintegration and ejection of large relatively cold chunks of material. At laser fluences close to the ablation threshold, the mechanical fracture is localized at a certain depth under the surface that is defined by the balance between the tensile stresses that are increasing with depth and the decreasing thermal softening due to the laser heating. At higher laser fluences material can lose its integrity over a larger surface region.

The differences in the mechanisms of material ejection in the regimes of thermal and stress confinement are reflected in the parameters of the ablation process accessible for experimental investigation. In particular, the amplitudes and the shape of the acoustic wave propagating from the absorption region are sensitive to changes in the mechanisms of material ejection and can be used for tuning the irradiation parameters to the desired ejection conditions. Much stronger acoustic waves are generated in the regime of stress confinement. Moreover, the shapes of the pressure profiles recorded in the stress confinement regime for desorption and ablation are substantially different from one another. A bipolar thermoelastic wave results from the interaction of the laser-induced compressive pressure with the free surface of the irradiated sample in the desorption regime, whereas formation of a strong unipolar compressive wave is characteristic of ablation. The fluence dependence of the amplitude of the tensile component of the pressure wave has a sharp maximum at the threshold fluence, providing an additional way for threshold identification in the stress confinement regime.

A comparison analysis of the plume composition and the velocities of ejected species in the stress and thermal confinement regimes has also revealed a number of differences that can have important implications for practical applications of laser ablation. Larger and more numerous clusters with higher ejection velocities are produced at the same laser fluences in the regime of stress confinement than in the regime of thermal confinement. For monomer molecules, ejection in the stress confinement regime result in broader velocity distributions in the direction normal to the irradiated surface, higher maximum velocities, and stronger forward peaking of the angular distributions.

The yield of monomers commonly measured in mass spectrometry experiments, on the contrary, appears to be not sensitive to the irradiation conditions. The fluence dependencies of the number of ejected monomers are nearly identical in the regimes of thermal and stress confinement. Moreover, the drastic increase of the total yield at the ablation thresholds is imperceptible from the yields of monomers that deceptively follow an Arrhenius-type dependence even in the high fluence region, where ablation occurs. In general, simulation results demonstrate that an extensive experimental study involving simultaneous detection of cluster and monomer yields, probing different parameters of the ejected plume, as well as photoacoustic measurement of the laser-induced pressure waves are needed to ensure a reliable interpretation of the mechanisms of molecular ejection.

ACKNOWLEDGMENTS

This work was supported by the United States Office of Naval Research through the Medical Free Electron Laser Program and the National Science Foundation through the Chemistry Division. The computational support was provided by IBM through the Selected University Research Program, the National Science Foundation through the MRI Program, and the Center for Academic Computing at Penn State University.

[1] M. Karas, in *Fundamental Processes in Sputtering of Atoms and Molecules*, edited by P. Sigmund (Det Kongelige Danske Videnskabernes Selskab, Copenhagen, 1993), p. 623.

[2] A. Vertes and R. Gijbels, in *Laser Ionization Mass Analysis*, edited by A. Vertes, R. Gijbels, and F. Adams (Wiley, New York, 1993), p. 127.
[3] R. E. Johnson, in *Large Ions: Their Vaporization, Detection and Structural Analysis*, edited by T. Baer, C. Y. Ng, and I. Powis (Wiley, New York, 1996), p. 49.
[4] *Laser–Tissue Interaction IX*, edited by S. L. Jacques, SPIE Proc. Series Vol. 3254 (SPIE, Bellingham, WA, 1998).
[5] S. L. Jacques, Appl. Opt. **32**, 2447 (1993).
[6] L. V. Zhigilei and B. J. Garrison, Appl. Phys. Lett. **74**, 1341 (1999).
[7] A. Miotello and R. Kelly, Appl. Phys. A: Mater. Sci. Process. **69A**, S67 (1999).
[8] R. Kelly and A. Miotello, Phys. Rev. E **60**, 2616 (1999).
[9] M. M. Martynyuk, Sov. Phys. Tech. Phys. **21**, 430 (1976).
[10] L. V. Zhigilei, P. B. S. Kodali, and B. J. Garrison, Chem. Phys. Lett. **276**, 269 (1997).
[11] K. Dreisewerd, M. Schürenberg, M. Karas, and F. Hillenkamp, Int. J. Mass Spectrom. Ion Processes **141**, 127 (1995).
[12] K. Dreisewerd, M. Schürenberg, M. Karas, and F. Hillenkamp, Int. J. Mass Spectrom. Ion Processes **154**, 171 (1996).
[13] M. Schürenberg, K. Dreisewerd, S. Kamanabrou, and F. Hillenkamp, Int. J. Mass Spectrom. Ion Processes **172**, 89 (1998).
[14] T. Huth-Fehre and C. H. Becker, Rapid commun. Mass Spectrom. **5**, 378 (1991).
[15] J. W. Elam and D. H. Levy, J. Phys. Chem. B **102**, 8113 (1998).
[16] A. Karabutov, N. Podymova, and V. Letokhov, Proc. SPIE **2624**, 93 (1996).
[17] M. Handschuh, S. Nettesheim, and R. Zenobi, Surf. Sci. **137**, 125 (1999).
[18] S. M. Hankin and P. John, J. Phys. Chem. B **103**, 4566 (1999).
[19] K. H. Song and X. Xu, Appl. Surf. Sci. **127–129**, 111 (1998).
[20] J. Heitz and J. T. Dickinson, Appl. Phys. A: Mater. Sci. Process. **68A**, 515 (1999).
[21] L. V. Zhigilei, P. B. S. Kodali, and B. J. Garrison, J. Phys. Chem. B **101**, 2028 (1997); **102**, 2845 (1998).
[22] Ł. Dutkiewicz, R. E. Johnson, A. Vertes, and R. Pędrys, J. Phys. Chem. A **103**, 2925 (1999).
[23] E. Ohmura and I. Fukumoto, Int. J. Jpn. Soc. Precis. Eng. **30**, 128 (1996).
[24] R. Srinivasan and B. Braren, Chem. Rev. **89**, 1303 (1989).
[25] Y. Tsuboi, K. Hatanaka, H. Fukumura, and H. Masuhara, J. Phys. Chem. A **102**, 1661 (1998).
[26] A. A. Oraevsky, S. L. Jacques, and F. K. Tittel, J. Appl. Phys. **78**, 1281 (1995).
[27] G. Paltauf and H. Schmidt-Kloiber, Appl. Phys. A: Mater. Sci. Process. **62A**, 303 (1996).
[28] D. Kim and C. P. Grigoropoulos, Appl. Surf. Sci. **127–129**, 53 (1998).
[29] D. E. Hare, J. Franken, and D. D. Dlott, J. Appl. Phys. **77**, 5950 (1995).
[30] I. Itzkan, D. Albagli, B. J. Banish, M. Dark, C. von Rosenberg, L. T. Perelman, G. S. Janes, and M. S. Feld, AIP Conf. Proc. **288**, 491 (1994).
[31] D. Albagli, L. T. Perelman, G. S. Janes, C. von Rosenberg, I. Itzkan, and M. S. Feld, Lasers Life Sci. **6**, 55 (1994).
[32] A. A. Oraevsky, R. Esenaliev, S. L. Jacques, and F. K. Tittel, Proc. SPIE **2391,** 300 (1995).
[33] R. Cramer, R. F. Haglund, Jr., and F. Hillenkamp, Int. J. Mass Spectrom. Ion Processes **169/170**, 51 (1997).
[34] R. S. Dingus and R. J. Scammon, Proc. SPIE **1427**, 45 (1991).
[35] V. Venugopalan, Proc. SPIE **2391**, 184 (1995).
[36] I. Itzkan, D. Albagli, M. L. Dark, L. T. Perelman, C. von Rosenberg, and M. S. Feld, Proc. Natl. Acad. Sci. USA **92**, 1960 (1995).
[37] For complex materials, such as soft tissues, the time of mechanical equilibration can be significantly longer than the one predicted by this simple acoustic approximation; see Refs. 30 and 35.
[38] T. Antoun, L. Seaman, and M. E. Glinsky, Proc. SPIE **2391**, 413 (1995).
[39] R. L. Webb, J. T. Dickinson, and G. J. Exarhos, Appl. Spectrosc. **51**, 707 (1997).
[40] *Laser Ablation and Desorption*, edited by J. C. Miller and R. F. Haglund, Jr. (Academic, London, 1998).
[41] L. V. Zhigilei and B. J. Garrison, Appl. Surf. Sci. **127–129**, 142 (1998); Proc. SPIE **3254**, 135 (1998).
[42] L. V. Zhigilei and B. J. Garrison, Mater. Res. Soc. Symp. Proc. **538**, 491 (1999).
[43] L. V. Zhigilei and B. J. Garrison, Appl. Phys. Lett. **71**, 551 (1997).
[44] L. V. Zhigilei and B. J. Garrison, Rapid Commun. Mass Spectrom. **12**, 1273 (1998).
[45] S. Woutersen and H. J. Bakker, Nature (London) **402**, 507 (1999).
[46] H. Kim and D. Dlott, J. Chem. Phys. **94**, 8203 (1991).
[47] R. E. Wyatt, C. Iung, and C. Leforestier, Acc. Chem. Res. **28**, 423 (1995).
[48] B. J. Garrison and R. Srinivasan, J. Appl. Phys. **57**, 2909 (1985).
[49] D. Fenyö, B. U. R. Sundqvist, B. R. Karlsson, and R. E. Johnson, Phys. Rev. B **42**, 1895 (1990).
[50] Y. G. Yingling, L. V. Zhigilei, and B. J. Garrison (unpublished).
[51] J. I. Etcheverry and M. Mesaros, Phys. Rev. B **60**, 9430 (1999).
[52] R. E. Rudd and J. Q. Broughton, Phys. Rev. B **58**, R5893 (1998).
[53] J. A. Smirnova, L. V. Zhigilei, and B. J. Garrison, Comput. Phys. Commun. **118**, 11 (1999).
[54] V. A. Likhachev, A. I. Mikhailin, and L. V. Zhigilei, Philos. Mag. A **69**, 421 (1994).
[55] D. A. Allwood, R. W. Dreyfus, I. K. Perera, and P. E. Dyer, Rapid Commun. Mass Spectrom. **10**, 1575 (1996).
[56] The initial temperature is zero in the simulations presented in this work. Results from the simulations with initial temperature of 500 K do support the physical picture of the material ejection discussed in Secs. III and IV. These results are presented in a separate paper, L. V. Zhigilei and B. J. Garrison, Appl. Phys. A: Mater. Sci. Process. **69A**, S75 (1999).
[57] R. E. Johnson and B. U. R. Sundqvist, Rapid Commun. Mass Spectrom. **5**, 574 (1991).
[58] Animated sequences of snapshots from the simulations discussed in this paper can be viewed at http://galilei.chem.psu.edu/~leo/ablation/animations/
[59] J. Sunner, M. G. Ikonomou, and P. Kebarle, Int. J. Mass Spectrom. Ion Processes **82**, 221 (1988).
[60] R. Kelly and A. Miotello, Appl. Surf. Sci. **96–98**, 205 (1996).
[61] M. Karas, M. Glückmann, and J. Schäfer, J. Mass Spectrom. **35**, 1 (2000).
[62] J. Shiea and J. Sunner, in *Methods and Mechanisms for Producing Ions from Large Molecules*, edited by K. G. Standing and W. Ens, NATO ASI Series 269 (Plenum, New York, 1991), p. 147.
[63] E. Dekel, S. Eliezer, Z. Henis, E. Moshe, A. Ludmirsky, and I. B. Goldberg, J. Appl. Phys. **84**, 4851 (1998).
[64] P. R. Williams, P. M. Williams, S. W. J. Brown, and H. N. V. Temperley, Proc. R. Soc. London, Ser. A **455**, 3311 (1999).
[65] N. J. Wagner, B. L. Holian, and A. F. Voter, Phys. Rev. A **45**, 8457 (1992).
[66] M. Glückmann and M. Karas, J. Mass Spectrom. **34**, 467 (1999).
[67] P. Demirev, A. Westman, C. T. Reiman, P. Håkansson, D. Barofsky, B. U. R. Sundqvist, Y. D. Cheng, W. Seibt, and K. Siegbahn, Rapid Commun. Mass Spectrom. **6**, 187 (1992).
[68] L. D. Landau and E. M. Lifshitz, *Fluid Mechanics* (Pergamon, New York, 1987)
[69] W. Zhang and B. T. Chait, Int. J. Mass Spectrom. Ion Processes **160**, 259 (1997).
[70] A. A. Puretzky, D. B. Geohegan, G. B. Hurst, M. V. Buchanan, and B. S. Luk'yanchuk, Phys. Rev. Lett. **83**, 444 (1999).
[71] S. Georgiou, A. Koubenakis, J. Labrakis, and M. Lassithiotaki, J. Chem. Phys. **109**, 8591 (1998).
[72] A. Koubenakis, T. Elimioti, and S. Georgiou, Appl. Phys. A: Mater. Sci. Process. **69A**, S637 (1999).
[73] D. Sibold and H. M. Urbassek, Phys. Rev. A **43**, 6722 (1991).
[74] R. Kelly, J. Chem. Phys. **92**, 5047 (1990).
[75] V. Venugopalan, N. S. Nishioka, and B. B. Mikić, Biophys. J. **69**, 1259 (1995).